Determination of methyl $^{13}C-^{15}N$ dipolar couplings in peptides and proteins by three-dimensional and four-dimensional magic-angle spinning solid-state NMR spectroscopy

Jonathan J. Helmus, Philippe S. Nadaud, Nicole Höfer,[a] and Christopher P. Jaroniec[b]
Department of Chemistry, The Ohio State University, Columbus, Ohio 43210, USA

(Received 8 August 2007; accepted 30 October 2007; published online 1 February 2008)

We describe three- and four-dimensional semiconstant-time transferred echo double resonance (SCT-TEDOR) magic-angle spinning solid-state nuclear magnetic resonance (NMR) experiments for the simultaneous measurement of multiple long-range $^{15}N-^{13}C^{methyl}$ dipolar couplings in uniformly ^{13}C, ^{15}N-enriched peptides and proteins with high resolution and sensitivity. The methods take advantage of ^{13}C spin topologies characteristic of the side-chain methyl groups in amino acids alanine, isoleucine, leucine, methionine, threonine, and valine to encode up to three distinct frequencies ($^{15}N-^{13}C^{methyl}$ dipolar coupling, ^{15}N chemical shift, and $^{13}C^{methyl}$ chemical shift) within a single SCT evolution period of initial duration $\sim 1/{}^1J_{CC}$ (where ${}^1J_{CC} \approx 35$ Hz, is the one-bond $^{13}C^{methyl}-^{13}C$ *J*-coupling) while concurrently suppressing the modulation of NMR coherences due to $^{13}C-^{13}C$ and $^{15}N-^{13}C$ *J*-couplings and transverse relaxation. The SCT-TEDOR schemes offer several important advantages over previous methods of this type. First, significant (approximately twofold to threefold) gains in experimental sensitivity can be realized for weak $^{15}N-^{13}C^{methyl}$ dipolar couplings (corresponding to structurally interesting, ~ 3.5 Å or longer, distances) and typical $^{13}C^{methyl}$ transverse relaxation rates. Second, the entire SCT evolution period can be used for $^{13}C^{methyl}$ and/or ^{15}N frequency encoding, leading to increased spectral resolution with minimal additional coherence decay. Third, the experiments are inherently "methyl selective," which results in simplified NMR spectra and obviates the use of frequency-selective pulses or other spectral filtering techniques. Finally, the $^{15}N-^{13}C$ cross-peak buildup trajectories are purely dipolar in nature (i.e., not influenced by *J*-couplings or relaxation), which enables the straightforward extraction of $^{15}N-^{13}C^{methyl}$ distances using an analytical model. The SCT-TEDOR experiments are demonstrated on a uniformly ^{13}C, ^{15}N-labeled peptide, N-acetyl-valine, and a 56 amino acid protein, B1 immunoglobulin-binding domain of protein G (GB1), where the measured $^{15}N-^{13}C^{methyl}$ dipolar couplings provide site-specific information about side-chain dihedral angles and the packing of protein molecules in the crystal lattice. © *2008 American Institute of Physics*.
[DOI: 10.1063/1.2817638]

I. INTRODUCTION

The past several years have witnessed rapid advances in magic-angle spinning (MAS) solid-state nuclear magnetic resonance (SSNMR) spectroscopy and its application to the detailed characterization of protein structure, dynamics, and function.[1] These advances, which include the availability of high field magnets, improved probe designs,[2,3] novel radio-frequency (rf) pulse schemes,[4,5] and general protocols for the preparation of optimal samples for SSNMR studies,[6–9] have enabled complete or nearly complete ^{13}C and ^{15}N sequential resonance assignments to be obtained for a number of uniformly ^{13}C, ^{15}N ($U-^{13}C$, ^{15}N) enriched proteins between $\sim 50-150$ amino acids.[9–19] The ability to perform quantitative SSNMR measurements on $U-^{13}C$, ^{15}N-labeled samples has also facilitated the determination of several *de novo* three-dimensional peptide and protein structures,[16,20–24] atomic-resolution studies of protein-protein interfaces,[25,26] protein hydration,[27–29] and protein backbone and side-chain dynamics[30–32] in microcrystalline proteins, as well as detailed studies of biological solids lacking long-range order, including supramolecular peptide and protein aggregates and membrane-bound proteins.[23,24,33–38]

While optimal SSNMR approaches for backbone and side-chain ^{13}C and ^{15}N assignments (which can be used to predict protein secondary structure[39]) are continuously being developed,[40–42] a suite of two-dimensional (2D) and three-dimensional (3D) triple-resonance experiments, based on SPECIFIC $^{15}N-^{13}C$ cross polarization[43] and a variety of $^{13}C-^{13}C$ magnetization transfer schemes (e.g., NCACX, NCOCX, CONCA, etc.),[4,5] provides an excellent starting point toward achieving complete sequential assignments of spectra for small—to medium-sized $U-^{13}C$, ^{15}N labeled proteins. These experiments can also be readily extended to provide site-specific information about relative orientations of various dipolar tensors in proteins,[44–46] thereby enabling a more precise definition of the secondary structure elements.

[a]On leave from the Department of Chemical and Environmental Sciences, University of Limerick, Limerick, Ireland.
[b]Author to whom correspondence should be addressed. Tel.: (614) 247-4284. Fax: (614) 292-1685. Electronic mail: jaroniec@chemistry.ohio-state.edu.

To establish the exact side-chain conformations and the global protein fold, however, additional data are required,[47] typically in the form of interatomic distance restraints r_{IS}, determined using methods which report on the magnitude of through-space magnetic dipole-dipole couplings D_{IS} between the nuclei ($D_{IS} \propto \gamma_I \gamma_S / r_{IS}^3$, where γ_I and γ_S are the gyromagnetic ratios of the coupled I and S spins).

SSNMR methods for restoring (or recoupling) dipole-dipole interactions in isolated homo- and heteronuclear spin-1/2 pairs under MAS (where they are effectively averaged) are well established,[48,49] and their applications to distance measurements in biological solids have been thoroughly discussed.[50,51] However, the direct application of most of these techniques to U−^{13}C, ^{15}N-enriched molecules, where virtually all ^{13}C and ^{15}N nuclei experience multiple through-space (D_{IS}) and through-bond (J_{IS}) couplings to the neighboring spins, poses significant challenges because the largest couplings in the cluster typically dominate the spin dynamics and can interfere with the accurate determination of weaker, structurally interesting dipolar couplings. Depending on the NMR experiment (i.e., the exact form of the effective spin Hamiltonian active during the recoupling period), the detrimental effects of the omnipresent one- and two-bond ^{13}C−^{13}C and ^{13}C−^{15}N couplings can range from the complication of magnetization transfer pathways leading to degraded spectral resolution and sensitivity[52,53] to the complete quenching of magnetization transfer via the weaker couplings.[54–56] Nevertheless, despite the relatively complex nature of multispin systems, significant progress has been made in the recent years in the development of SSNMR methods for the accurate determination of weak ^{13}C−^{13}C (Refs. 57–64) and ^{13}C−^{15}N (Refs. 52 and 65–71) dipolar couplings in U−^{13}C, ^{15}N-labeled molecules. We note that complementary techniques have been proposed to derive multiple qualitative/semiquantitative distance restraints in U−^{13}C, ^{15}N-labeled proteins based on the measurement of ^{1}H−^{1}H (Refs. 16, 27, and 72–74) and ^{13}C−^{13}C (Refs. 14, 21, 22, and 53) couplings (and very recently also nuclear pseudocontact shifts[75] or enhanced transverse relaxation rates[76] in paramagnetic proteins).

Here, we focus on SSNMR methods for the quantitative measurement of multiple long-range ^{13}C−^{15}N dipolar couplings in U−^{13}C, ^{15}N-labeled proteins. Specifically, we are interested in multidimensional NMR schemes, which enable the simultaneous measurement of *all* ^{13}C−^{15}N couplings in U−^{13}C, ^{15}N molecules with arbitrary ^{13}C and ^{15}N chemical shifts. One such scheme, proposed by Michal and Jelinski[66] and subsequently extended by Jaroniec *et al.*[52] corresponds to a 3D "out-and-back-type"[77] pulse sequence based on the experimentally highly robust[78,79] (and closely related) rotational echo double resonance[80] (REDOR) and transferred echo double resonance[81] (TEDOR) techniques. This 3D TEDOR scheme combines two independent frequency-labeling periods, t_1(^{15}N) and t_2(^{13}C), for site-specific resolution, with REDOR-type ^{13}C−^{15}N dipolar coherence transfers (where the duration of the coherence-transfer periods is incremented in the third dimension, τ_{CN}, to encode distance information into ^{15}N−^{13}C cross-peak intensities). Note that although all dipolar couplings between a particular ^{13}C (denoted here as C) and the neighboring ^{15}N nuclei ($N_i, N_j, N_k, \ldots$) are simultaneously restored during 3D TEDOR, the typical ^{15}N−^{13}C cross-peak buildup trajectories depend primarily on the magnitude of the active ^{15}N−^{13}C dipolar coupling (i.e., the coupling C−N_i responsible for the cross peak at isotropic chemical shifts [Ω_{N_i}, Ω_C] in the 2D correlation map) and only to a lesser extent on the passive couplings to all other ^{15}N (i.e., C−N_j, C−N_k, etc.).[52] Two significant problems related to spectral resolution and sensitivity hinder the extension of the broadband (and most generally applicable) version of the 3D TEDOR scheme (z-filtered TEDOR or ZF-TEDOR[52]) from peptides to larger U−^{13}C, ^{15}N-labeled proteins. First, the ^{15}N−^{13}C cross peaks are modulated by ~30–60 Hz one-bond ^{13}C−^{13}C J-couplings ($^1J_{CC}$), which leads to reduced cross-peak intensities by limiting the useful ^{15}N−^{13}C coherence-transfer times to only ~8–14 ms (Ref. 52) (ideally, longer times, at least ~16–20 ms, are desirable to achieve significant coherence transfer via weak ^{15}N−^{13}C couplings). Second, the resolution is limited by the 2D ^{15}N−^{13}C correlation spectrum, which may become highly congested for larger systems (especially since multiple ^{15}N−^{13}C cross peaks are obtained for each ^{13}C site). While relatively straightforward solutions to both of these problems can be (or have been) proposed, these solutions have serious drawbacks that limit their general utility, as discussed below. For example, a band-selective 3D TEDOR experiment, where ^{13}C−^{13}C J-couplings to ^{13}C spins of interest are suppressed using frequency-selective pulses, has been developed.[52] However, this scheme is limited by the chemical shift dispersion and is applicable only to certain types of ^{13}C sites (e.g., decoupling of $^{13}C'-^{13}C\alpha$ J-couplings for all protein residues is straightforward, but the suppression of $^{13}C\gamma-^{13}C\delta$ couplings for leucines, $^{13}C\alpha-^{13}C\beta$ for serines, etc., is, in general, difficult or even impossible to achieve due to similar chemical shifts of the coupled ^{13}C nuclei). The limited spectral resolution problem can also, in principle, be easily addressed by appending to the existing 3D ZF-TEDOR scheme an additional ^{13}C chemical shift evolution period followed by a ^{13}C−^{13}C magnetization transfer sequence [thus converting it into a four-dimensional (4D) NMR experiment]. In practice, however, this approach, which would further extend the duration of the (already relatively long) pulse sequence by another ~10–15 ms, will generally be associated with additional sensitivity losses due to spin relaxation and ^{13}C−^{13}C J-modulation of the NMR signals.

In this paper, we present 3D and 4D semiconstant-time TEDOR (SCT-TEDOR) NMR pulse schemes, which, for certain common amino acid ^{13}C spin topologies, effectively circumvent the aforementioned problems and enable the simultaneous measurement of multiple long-range ^{15}N−^{13}C distances in U−^{13}C, ^{15}N-labeled proteins with high resolution and sensitivity. Although the methods can be readily applied to any type of ^{13}C site, which experiences a single one-bond J-coupling to another ^{13}C nucleus (e.g., $^{13}C'$, $^{13}C^{methyl}$, etc.) (or is not strongly J coupled), we believe that the most general and useful application of this methodology will be to ^{13}C methyl groups of alanine, isoleucine, leucine, methionine, threonine, and valine, and here we focus exclu-

sively on this application. Methyl groups are highly sensitive probes of protein structure and dynamics, and have been at the forefront of some of the most exciting developments in solution-state NMR methodology for studies of high molecular weight proteins[82] and also recently in biomolecular solid-state NMR.[83,84] These groups are over-represented in proteins in general and in membrane proteins in particular: The six methyl group containing amino acids (Ala, Ile, Leu, Met, Thr, and Val) correspond to 30% of the 20 naturally occurring amino acids, but account for over 37% of the database of more than 1000 unrelated proteins of known sequence,[85] and comprise ~50%–60% of residues found in membrane proteins[86–88] [in the B1 immunoglobulin-binding domain of protein G (GB1) used in this study, these six residues account for nearly 45% of the sequence]. Moreover, methyl groups are usually quite well dispersed throughout the primary sequence[89] and play significant roles in defining the structure of hydrophobic protein cores,[82] functional dynamics,[90] ligand binding,[84] and long-range intermolecular interactions in supramolecular peptide aggregates.[33,91,92]

The new SCT-TEDOR methods take advantage of the characteristic ^{13}C spin topology of side-chain methyl groups in Ala, Ile, Leu, Thr, Val [single $^1J_{CC}$ of ~35 Hz (Ref. 77)], and Met [$^1J_{CC}=0$, $^2J_{CC}/^3J_{CC} \lesssim 4$ Hz (Ref. 93)] to encode up to three distinct frequencies ($^{15}N-^{13}C^{methyl}$ dipolar coupling, ^{15}N chemical shift, and $^{13}C^{methyl}$ chemical shift) within a single SCT evolution period of initial duration $\sim 1/^1J_{CC} \approx 28$ ms (typical total duration up to ~35 ms) while concurrently suppressing the modulation of NMR coherences due to $^{13}C-^{13}C$ and $^{15}N-^{13}C$ J-couplings and transverse relaxation. The utilization of the entire SCT period for $^{13}C^{methyl}$ and/or ^{15}N chemical shift encoding leads to very high spectral resolution without major sensitivity compromises and is facilitated by a period of $^{15}N-^{13}C^{methyl}$ multiple-quantum (i.e., zero- and double-quantum coherence) evolution to encode the ^{15}N frequency, bracketed by two identical periods, during which concurrent $^{15}N-^{13}C^{methyl}$ coherence transfer and $^{13}C^{methyl}$ frequency labeling of single-quantum/antiphase coherences can take place. Note that at the fundamental level, the SCT-TEDOR sequences described here are the dipolar $^{13}C-^{15}N$ SSNMR analogs of the well-known heteronuclear multiple-quantum coherence experiment in solution,[94,95] further modified using schemes designed to enhance spectral resolution and sensitivity.[96–100] We show in a model U–^{13}C, ^{15}N labeled peptide, N-acetyl-valine, and a 56-residue protein, GB1, that in addition to improved resolution, SCT-TEDOR can offer significant (up to approximately twofold to threefold) gains in sensitivity for measurements of weak $^{15}N-^{13}C^{methyl}$ dipolar couplings (corresponding to ~3.5 Å or longer distances), and that inherently these schemes are "methyl selective," which results in simplified NMR spectra and obviates the use of frequency-selective pulses[52] or other spectral filtering techniques.[101] Moreover, since the $^{15}N-^{13}C$ cross-peak buildup trajectories are purely dipolar in nature (i.e., not influenced by J-couplings or relaxation), the $^{15}N-^{13}C^{methyl}$ distances can be easily extracted using an analytical model. Finally, we note that with the exception of intraresidue $^{15}N-^{13}C\beta$ correlations for alanine, all other cross peaks report on nontrivial, structurally interesting $^{15}N-^{13}C^{methyl}$ distances and, in general, provide valuable site-specific information about side-chain dihedral angles and three-dimensional protein structure.

II. MATERIALS AND METHODS

A. Sample preparation

The U–^{13}C, ^{15}N-labeled N-acetyl-valine (NAV) sample, which consisted of 20% U–^{13}C, ^{15}N-NAV diluted in natural abundance NAV by recrystallization from aqueous methanol (to reduce intermolecular $^{13}C-^{15}N$ contacts), was a kind gift from Rienstra (University of Illinois, Urbana-Champaign). The sample was center packed in a 3.2 mm 22 μl rotor (Varian Inc., Palo Alto, CA) to minimize the effects of rf inhomogeneity.

U–^{13}C, ^{15}N-labeled GB1 was prepared using standard molecular biology techniques. *E. coli* BL21(DE3) cells were transformed with the plasmid corresponding to the T2Q mutant of GB1 (kindly provided by Gronenborn, University of Pittsburgh), grown at 37 °C on a minimal medium containing 1 g/l $^{15}NH_4Cl$ and 3 g/l ^{13}C-glucose, and supplemented with 10 ml of 10× ^{13}C, ^{15}N-labeled Bioexpress cell growth medium (Cambridge Isotope Laboratories, Andover, MA). Protein expression was induced at OD_{600} of ~0.6 by the addition of isopropyl β-D-thiogalactoside to a final concentration of 0.5 mM, and cell growth was continued for 4 h. Cells were harvested by centrifugation at 4000g for 20 min at 4 °C, and cell lysis was achieved using lysozyme digestion followed by ultrasonication. Specifically, the cell pellet from a 1 L culture was resuspended in 25 ml of the lysis buffer (50 mM tris·HCl, 300 mM NaCl, pH 8) containing 5 mM $MgCl_2$, 1 mM $CaCl_2$, ~300 units of DNAse I (Invitrogen, Carlsbad, CA), ~35 units of RNAse A (Qiagen Inc., Valencia, CA), 1 mg/ml lysozyme (American Bioanalytical, Natick, MA), and ~0.1% Triton X-100 (Sigma-Aldrich, St. Louis, MO), and incubated on ice with stirring for 1 h. The cell suspension was subsequently ultrasonicated on ice and centrifuged at 45 000g for 30 min at 4 °C to remove the cell debris. In a final prepurification step, the supernatant containing GB1 was heated at 80 °C for 10 min, centrifuged at 45 000g for 30 min at 4 °C, and concentrated using an Amicon Ultra-15 centrifugal 5000 molecular weight cut-off (MWCO) filter unit (Millipore, Billerica, MA). GB1 was purified by fast protein liquid chromatography (FPLC) using a HiLoad 16/60 Superdex 75 prep grade column (Amersham Biosciences/GE Healthcare) equilibrated with a 50 mM sodium phosphate, 150 mM NaCl, and pH 6.5 buffer. Peak fractions containing the protein were pooled, concentrated using an Amicon 5000 MWCO filter, washed extensively with 50 mM sodium phosphate and pH 6.5 buffer and concentrated to a final protein concentration of 30 mg/ml. Typical yields of purified GB1 obtained using this procedure were ~100 mg/l of cell culture.

GB1 microcrystals for SSNMR studies were prepared according to the published batch precipitation procedure.[15] Briefly, a total of 1.2 ml of 2:1 (v/v) solution of 2-methylpentane-2,4-diol:isopropanol was added in three aliquots to 0.4 ml of the 30 mg/ml GB1 solution (i.e., 12 mg of

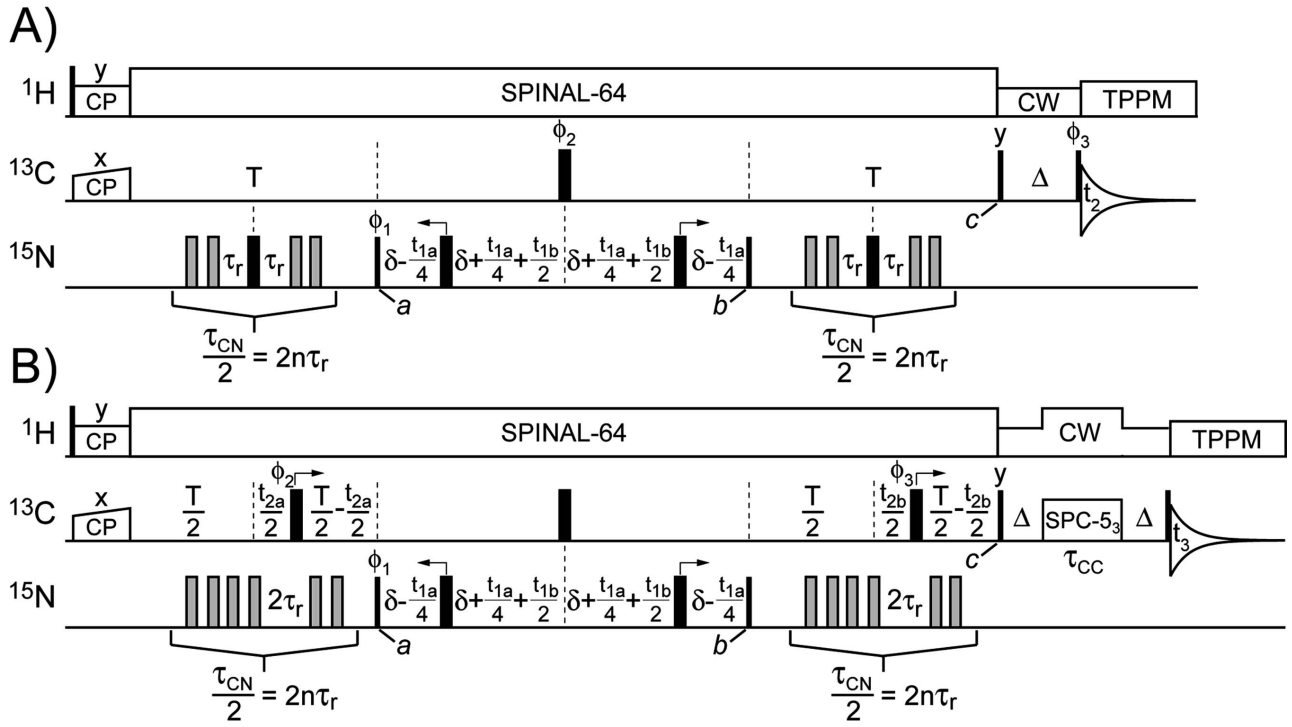

FIG. 1. Pulse schemes of the (A) 3D and (B) 4D semiconstant-time TEDOR (SCT-TEDOR) experiments. Narrow and wide black rectangles correspond to 90° and 180° pulses, and have phase x unless indicated otherwise. The REDOR 180° ^{15}N pulses (filled gray rectangles) were phase cycled according to the xy-4 scheme (Ref. 78). Typical parameters used to record the GB1 spectra are given below (see text for additional details and pulse sequence description). The ^{1}H, ^{13}C, and ^{15}N carriers were placed at 4.7, 30, and 120 ppm, respectively, and for both schemes the delays were Δ=6.0 ms, T=11.88 ms, and δ=0.9 ms. These delay settings result in the initial duration of the semiconstant-time evolution period of $T_C=2T+4\delta\approx 1/{}^{1}J_{CC}=27.36$ ms, which effectively refocuses the methyl ^{13}C magnetization evolving under the ~35 Hz one-bond ^{13}C–^{13}C J-coupling, and enables up to $\sim 2T\approx 23.76$ ms of ^{13}C–^{15}N dipolar evolution (τ_{CN}) and constant-time ^{13}C chemical shift evolution (t_2) (4D pulse scheme only), and up to $\sim 4\delta$=3.6 ms of constant-time ^{15}N chemical shift evolution (t_1). Scheme (A), 3D SCT-TEDOR: The semiconstant-time ^{15}N frequency labeling during t_1 was accomplished as follows. First, the two ^{15}N refocusing 180° pulses (initially placed in the center of the two periods of duration 2δ) were moved *simultaneously* in opposite directions by $t_{1a}/4$, as shown in the figure (this implementation enables ^{15}N chemical shift encoding, while refocusing all ^{15}N–^{13}C J-couplings for each t_1 increment). Subsequently, once the entire 4δ period has been used (i.e., the 180° ^{15}N pulses can no longer be moved), the ^{15}N frequency-labeling period can be extended further (typically by an additional ~4–8 ms, limited primarily by the dephasing of ^{15}N–^{13}C$^{\text{methyl}}$ multiple-quantum coherence generated at time point a, under $^{1}J_{CC}$) by incrementing the variable delay t_{1b}, as indicated in the figure. In our implementation, each ^{15}N t_{1a} and t_{1b} increment (Δt_{1a} and Δt_{1b}) had the duration $\Delta t_{1a}=\Delta t_{1b}=360$ μs, and a total of 30 increments were recorded for a maximum ^{15}N evolution period of $t_{1,\max}$=10.44 ms (note that for experiments where τ_{CN} times up to ~16–18 ms are investigated, an alternative, purely constant-time implementation of the experiment may be preferable with the following typical parameters: T=8.28 ms, δ=2.7 ms, Δt_{1a}=360 μs, and Δt_{1b}=0). Phase cycling: $\phi_1=x,-x$; $\phi_2=2(x),2(y),2(-x),2(-y)$; $\phi_3=8(x),8(-x)$; receiver=$2(x,-x,-x,x)$, $2(-x,x,x,-x)$. Quadrature in the ^{15}N (F_1) dimension was achieved by phase cycling of ϕ_1 according to the method of States *et al.* (Ref. 121). Scheme (B), 4D SCT-TEDOR: Semiconstant-time ^{15}N chemical shift labeling was identical to that described in scheme (A). ^{13}C$^{\text{methyl}}$ constant-time frequency labeling was achieved by first incrementing the delay $t_{2a}/2$ up to ~$T/2$, followed by incrementing the delay $t_{2b}/2$, also up to ~$T/2$ (in our implementation, each ^{13}C t_2 increment was $\Delta t_{2a}=\Delta t_{2b}=90$ μs). Following the semiconstant-time evolution period encoding the ^{15}N and ^{13}C$^{\text{methyl}}$ chemical shifts, and ^{15}N–^{13}C$^{\text{methyl}}$ dipolar couplings during t_1, t_2, and τ_{CN}, respectively, ^{13}C–^{13}C magnetization transfer was achieved using an off-resonant band-selective SPC-5$_3$ pulse sequence (Refs. 54 and 108) (effective carrier frequency at 42 ppm), with a ^{13}C field strength of 37 kHz and duration of τ_{CC}=1.35 ms ($15\tau_r$). Phase cycling: $\phi_1=x,-x$; $\phi_2=2(x),2(y)$; $\phi_3=4(x),4(y)$; receiver=$x,-x,-x,x,-x,x,x,-x$. Quadrature in the ^{15}N (F_1) dimension was achieved by phase cycling of ϕ_1 according to the method of States *et al.* For quadrature in the ^{13}C (F_2) dimension, TPPI (Ref. 122) was applied to the initial ^{1}H 90° pulse and the ^{1}H and ^{13}C cross-polarization pulses.

protein) in 50 mM sodium phosphate, pH 6.5, and the microcrystal formation was allowed to proceed at room temperature for 1 h. The sample was centrifuged and the pellet center packed in a 3.2 mm 22 μl Varian rotor by centrifugation. The amount of U–^{13}C, ^{15}N-labeled GB1 in the final sample was ~10 mg (1.5 μmol). 1D ^{13}C and ^{15}N CPMAS, and 2D ^{13}C–^{13}C and ^{15}N–^{13}C correlation spectra were recorded to assess the microcrystal quality and to confirm the published GB1 assignments.[15]

B. NMR spectroscopy

NMR experiments were performed on a three-channel Varian spectrometer operating at the frequencies of 499.8 MHz for ^{1}H, 125.7 MHz for ^{13}C, and 50.6 MHz for ^{15}N, equipped with a T3 HXY 3.2 mm MAS probe. The MAS frequency of 11.111 kHz, regulated to approximately ±3 Hz, was used for all experiments. Sample temperature during experiments was controlled using a stream of dry compressed air, delivered to the sample via a variable-temperature (VT) stack at a flow rate of approximately 30 l/min. For NAV, the VT gas temperature was set to 293 K, resulting in an effective sample temperature (due to frictional heating) of approximately 298 K, as determined by lead nitrate calibration;[102] for GB1 the VT gas was set to 273 K, resulting in an effective sample temperature of approximately 278 K.

The 3D and 4D SCT-TEDOR pulse schemes are shown in Fig. 1. The detailed description of the pulse schemes is

provided in Sec. III below, and the key experimental parameters are given in the figure caption; only the standard parameters common to both schemes are given here. Note that proper rotor synchronization is essential for the successful implementation of these pulse schemes, and the parameters listed below and in the figure caption assume a MAS rate, $\omega_r/2\pi$, of 11.111 kHz (i.e., the rotor period $\tau_r=90$ μs). Unless indicated otherwise, the ^{1}H, ^{13}C, and ^{15}N 90° pulse lengths were 2.5, 3.0, and 5.0 μs, respectively. The ^{1}H–^{13}C cross polarization[103] (CP) was achieved using a constant ^{1}H field, $\omega_{rf}/2\pi$, of 65 kHz, a ^{13}C field of 52 ± 7 kHz (i.e., by matching the $n=-1$ Hartmann-Hahn condition) applied with a linear ramp profile,[104] and contact times of 1–2 ms. All ^{15}N 180° pulses during the REDOR ^{13}C–^{15}N dipolar mixing periods (τ_{CN}) [including the two ^{15}N refocusing pulses in the scheme of Fig. 1(A)] were applied at a field strength of 27.8 kHz (i.e., $t_{180}=18$ μs; $\omega_{rf}/\omega_r\approx2.5$). Throughout the entire SCT evolution period, with initial duration $T_C=2T+4\delta\approx1/{}^1J_{CC}$, SPINAL-64 ^{1}H decoupling[105] was applied at a 100 kHz field strength (pulse length of 4.9 μs, total phase difference of 10.5°); the optimal decoupling parameters were obtained by maximizing the absolute ^{13}C spin-echo intensity using the standard spin-echo pulse sequence[106] on the ^{13}C channel: CP-$T_C/2$-180°-$T_C/2$-*z-filter-acquire*, with $T_C=27$ ms. During the *z*-filter periods of duration $\Delta=6$ ms, used for the suppression of transverse ^{13}C coherences, a 50 kHz cw ^{1}H field was applied (in our experience this provided an efficient suppression of transverse coherences, while concurrently minimizing ^{13}C–^{13}C magnetization transfer via proton-driven spin diffusion[107]), and 110 kHz cw proton decoupling was employed during SPC-5_3 band-selective ^{13}C–^{13}C double-quantum mixing[54,108] [pulse scheme in Fig. 1(B) only]. During acquisition, two-pulse phase modulated (TPPM) ^{1}H decoupling[109] was applied at a field strength of ~70 kHz (pulse length of 7.0 μs, total phase difference of 8.5°).

III. THEORETICAL BACKGROUND

A. Nuclear spin interactions in U–^{13}C, ^{15}N-labeled systems

For a U–^{13}C, ^{15}N-labeled solid rotating rapidly at the magic angle ($\theta_m=\tan^{-1}\sqrt{2}\approx54.7°$), far from ^{13}C–^{13}C and ^{15}N–^{15}N rotational resonance conditions,[57] and in the presence of efficient ^{1}H decoupling, the effective Hamiltonian describing the spin dynamics during the free evolution periods consists of terms corresponding to the isotropic chemical shifts, heteronuclear and homonuclear *J* couplings,

$$H=\sum_i \Omega_{C_i}C_{iz}+\sum_i \Omega_{N_i}N_{iz}+\sum_{i,j}\pi J^{ij}_{CN}2C_{iz}N_{jz}+\sum_{i<j}\pi J^{ij}_{CC}2C_{iz}C_{jz}. \quad (1)$$

In Eq. (1), the angular momentum operators representing ^{13}C and ^{15}N nuclei are denoted by C and N, respectively, Ω_C and Ω_N are the ^{13}C and ^{15}N isotropic chemical shifts, and J_{CN} and J_{CC} are the ^{13}C–^{15}N and ^{13}C–^{13}C *J*-coupling constants in hertz (assumed to be in the weak-coupling regime,[110] i.e., $|\Omega_1-\Omega_2|\gg|\pi J_{12}|$). During the REDOR coherence-transfer periods of length $\tau_{CN}/2$ (Fig. 1), the effective Hamiltonian nominally contains terms describing the recoupled ^{13}C–^{15}N dipolar interactions ω and ^{13}C–^{13}C *J*-couplings [we ignore, for the moment, the concurrent isotropic ^{13}C chemical shift evolution introduced intentionally in the pulse scheme of Fig. 1(B)]:

$$H=\sum_{i,j}\omega_{ij}2C_{iz}N_{jz}+\sum_{i<j}\pi J^{ij}_{CC}2C_{iz}C_{jz}, \quad (2)$$

where

$$\omega_{ij}=-2\sqrt{2}D_{ij}\sin(2\beta)\sin(\gamma) \quad (3)$$

and

$$D_{ij}=-\left(\frac{\mu_0}{4\pi}\right)\frac{\gamma_C\gamma_N\hbar}{2\pi r^3_{ij}}. \quad (4)$$

The Euler angles, β and γ, describe the orientation of the ^{13}C–^{15}N dipole vector in the rotor-fixed reference frame. The dipolar coupling constant *D* (in hertz) is a function of the characteristic ^{13}C and ^{15}N gyromagnetic ratios γ_C and γ_N and the internuclear distance *r*. We note here that the minor scaling of *D* due to the finite duration of the REDOR 180° pulses[111] can be ignored in the data analysis (under our experimental conditions, this leads to errors of <0.05 Å in the estimated ^{13}C–^{15}N distances, which are negligible relative to other sources of error, as discussed below).

B. 3D SCT-TEDOR pulse scheme

Since the effective Hamiltonian terms in Eqs. (1) and (2) commute with each other at all times, the evolution of spin coherences during the SCT-TEDOR experiments can be derived independently for each of the terms using straightforward product-operator calculations.[110] The basic spin dynamics during 3D-TEDOR-type experiments have been previously discussed in detail,[52,66] and we focus here on the unique features of the SCT-TEDOR schemes and their application to the simultaneous measurement of dipolar couplings between ^{15}N and methyl ^{13}C nuclei in U–^{13}C, ^{15}N-labeled molecules. The 3D SCT-TEDOR scheme [Fig. 1(A)] is described first in detail, and the discussion is subsequently extended to the 4D implementation of the method [Fig. 1(B)].

The transverse magnetization on the *i*th $^{13}C^{methyl}$ nucleus, denoted by the initial density operator $\rho(0)=C_{ix}$, is created using ^{1}H–^{13}C CP (note that although not employed in the experiments described here, nuclear Overhauser polarization techniques[112,113] can also be used to generate $^{13}C^{methyl}$ magnetization with potentially higher sensitivity than CP). Ignoring, for the moment, all rf irradiation on the ^{15}N channel and assuming $t_{1b}=0$, we note that the pulse sequence in Fig. 1(A) corresponds to a simple ^{13}C spin echo[106] with a total duration $T_C=2T+4\delta$ (followed, at time point *c*, by a *z*-filter of length Δ). During the spin-echo period, the only interaction leading to a significant, coherent spin evolution is the *J*-coupling between the methyl ^{13}C and the directly bonded aliphatic ^{13}C ($^1J_{CC}\approx35\pm2$ Hz for all methyl-containing residues, except Met where $^1J_{CC}=0$). Therefore, by setting $T_C\approx1/{}^1J_{CC}\approx28$ ms, as is commonly done in many solution-state NMR pulse schemes,[77] the one-bond

J-couplings involving methyl ^{13}C are essentially completely refocused during the constant-time period T_C (since $\cos(\pi^1 J_{CC} T_C) \approx -1$) and do not need to be considered further at this point.

Following $^1H-^{13}C$ CP, a REDOR sequence of duration $\tau_{CN}/2$, consisting of a rotor-synchronized train of 180° pulses [filled gray rectangles in Fig. 1(A)], is applied on the ^{15}N channel to recouple all $^{13}C-^{15}N$ dipolar couplings. The relevant density operator term (selected by the applied phase cycling and leading to observable magnetization during t_2), which is present immediately before the ^{15}N 90° pulse at time point a, corresponds to $^{13}C^{methyl}$ antiphase coherence,[77,110]

$$\rho(a^-) = 2C_{iy}N_{jz} \sin(\omega_{ij}\tau_{CN}/2) \prod_{k\neq j} \cos(\omega_{ik}\tau_{CN}/2), \tag{5}$$

where ω_{ij} is the active $^{15}N-^{13}C^{methyl}$ dipolar coupling and ω_{ik} are the passive couplings between the methyl ^{13}C and all other ^{15}N nuclei. Note that the REDOR pulses are applied symmetrically about the central 180° ^{15}N pulse (black rectangle), as shown in the figure, with a spacing of $\tau_r/2$ (although not absolutely critical to the experiment as far as the evolution of $^{13}C^{methyl}$ coherences is concerned, this particular implementation eliminates any spectral artifacts arising from magnetization transfer via the ~10–15 Hz $^{13}C'-^{15}N$ and $^{13}C\alpha-^{15}N$ one-bond J-couplings[77] for $\tau_{CN}/2=0$). Note also that the REDOR period has the duration of $\tau_{CN}/2=2n\tau_r$, where $n=0,1,2,\ldots$ [the $n=1$ case is shown in Fig. 1(A)], and does not include the $2\tau_r$ period containing the central 180° ^{15}N pulse (during which $^{13}C-^{15}N$ couplings are refocused).

At time point a, the 90° ^{15}N ϕ_1-pulse ($\phi_1=\pm x$ for coherence selection and, independently, $\phi_1=\pm y$ for quadrature detection in the F_1 dimension) converts the antiphase coherence into $^{13}C^{methyl}-^{15}N$ multiple-quantum coherence (MQC);[77,110] e.g., for $\phi_1=x$, we have

$$\rho(a^+) = -2C_{iy}N_{jy} \sin(\omega_{ij}\tau_{CN}/2) \prod_{k\neq j} \cos(\omega_{ik}\tau_{CN}/2). \tag{6}$$

The MQC ^{15}N frequency encoding takes place in t_{1a}, during the constant-time period 4δ (i.e., we assume $t_{1b}=0$ for the time being). Note that in this particular implementation, MQC evolution under all other interactions (i.e., $^{13}C^{methyl}$ chemical shift, $^{15}N-^{13}C'$, and $^{15}N-^{13}C\alpha$ J-couplings) is effectively suppressed. Moreover, the MQC formally does not evolve under $^{15}N-^{13}C^{methyl}$ dipolar and J-couplings[77,110] [although these interactions are generally negligible, with the dipolar coupling effectively averaged by MAS and $^{15}N-^{13}C^{methyl}$ $^2J_{NC}/^3J_{NC} < 2$ Hz (Ref. 114)]. Immediately before the 90° ^{15}N pulse at time point b, the density operator is

$$\rho(b^-) = -2C_{iy} \sin(\omega_{ij}\tau_{CN}/2) \prod_{k\neq j} \cos(\omega_{ik}\tau_{CN}/2) \times [N_{jy} \cos(\Omega_{N_j} t_{1a}) - N_{jx} \sin(\Omega_{N_j} t_{1a})]. \tag{7}$$

The 90° ^{15}N x-pulse selects the cosine Ω_{N_j}-modulated MQC component and converts it back into $^{13}C^{methyl}$ antiphase coherence,

$$\rho(b^+) = -2C_{iy}N_{jz} \sin(\omega_{ij}\tau_{CN}/2) \times \prod_{k\neq j} \cos(\omega_{ik}\tau_{CN}/2)\cos(\Omega_{N_j} t_{1a}), \tag{8}$$

which is subsequently transformed during the second REDOR period of duration $\tau_{CN}/2$ (identical to the first REDOR period) into observable $^{13}C^{methyl}$ single-quantum coherence at time point c,

$$\rho(c) = 2C_{ix} \sin^2(\omega_{ij}\tau_{CN}/2) \prod_{k\neq j} \cos^2(\omega_{ik}\tau_{CN}/2)\cos(\Omega_{N_j} t_{1a}). \tag{9}$$

This $^{13}C^{methyl}$ single-quantum coherence is converted into longitudinal magnetization ($\sim C_{iz}$) by the 90° ^{13}C y-pulse at time point c, stored along the z-axis during the short z-filter period of duration Δ (while any residual transverse ^{13}C coherences are dephased), returned to the transverse plane by the 90° ^{13}C ϕ_3-pulse, and detected during t_2. The final powder-averaged NMR signal, assuming the usual quadrature detection in F_1 and F_2 dimensions[77,110] and ignoring normalization constants, is given by

$$\begin{aligned} S(t_{1a},t_2,\tau_{CN}) &= \langle \mathrm{Tr}\{C_i^+ \rho(c)\}\rangle \\ &= \langle \sin^2(\omega_{ij}\tau_{CN}/2) \prod_{k\neq j} \cos^2(\omega_{ik}\tau_{CN}/2)\rangle \\ &\quad \times \exp(i\Omega_{N_j} t_{1a}) \exp(i\Omega_{C_i} t_2), \end{aligned} \tag{10}$$

where $\langle\ldots\rangle$ denotes the powder average. As stated qualitatively in the Introduction, Eq. (10) describes a cross peak at frequencies $[\Omega_{N_j}, \Omega_{C_i}]$ in the 2D $^{15}N-^{13}C$ NMR spectrum, which evolves due to the active $^{15}N-^{13}C^{methyl}$ dipolar coupling, ω_{ij} (the precise values of ω_{ij} depend on the orientation of the individual crystallites in the powder sample) as a function of the REDOR mixing time, τ_{CN}, according to $\sin^2(\omega_{ij}\tau_{CN}/2)$, and is further modulated as $\cos^2(\omega_{ik}\tau_{CN}/2)$ by the passive $^{15}N-^{13}C^{methyl}$ couplings, ω_{ik}.

The constant-time (CT) period, $T_C=2T+4\delta \approx 1/^1J_{CC} \approx 28$ ms, during which the one-bond $^{13}C^{methyl}-^{13}C^{aliphatic}$ J-coupling is effectively refocused, is used for both $^{13}C^{methyl}-^{15}N$ coherence transfer and ^{15}N frequency encoding. The optimal duration of the $^{13}C^{methyl}-^{15}N$ coherence-transfer period ($2T$) will typically be in the range, $2T \approx 16-24$ ms, which leaves a period of $4\delta \approx 4-12$ ms for CT ^{15}N chemical shift labeling. While for some experiments, this ^{15}N frequency-labeling period will be sufficient, it can be easily increased by an additional period of up to ~4–8 ms to enhance spectral resolution in the ^{15}N dimension, with minimal effect on spectral sensitivity. This is done by incrementing the variable delays $t_{1b}/2$ about the central ^{13}C 180° ϕ_2 pulse, as shown in Fig. 1(A), once the entire 4δ period has been used for ^{15}N frequency encoding (i.e., the moving 180° ^{15}N pulses are next to the 90° pulses and can no longer be moved). Note that the various parameters are set such that the t_{1a} and t_{1b} increments, Δt_{1a} and Δt_{1b}, respectively, are equal (Fig. 1). The final powder-averaged NMR signal for this SCT-TEDOR experiment is

$$S(t_1,t_2,\tau_{CN}) = \langle \sin^2(\omega_{ij}\tau_{CN}/2)\prod_{k\neq j}\cos^2(\omega_{ik}\tau_{CN}/2)\rangle \times \cos(\pi^1 J^{ij}_{CC} t_{1b})\exp(i\Omega_{N_j} t_1)\exp(i\Omega_{C_i} t_2), \quad (11)$$

where

$$t_1 = t_{1a} + t_{1b}. \quad (12)$$

Note that the factor $\cos(\pi\, {}^1J^{ij}_{CC} t_{1b})$ in Eq. (11), which describes the modulation of $^{15}N-{}^{13}C^{methyl}$ MQC due to the one-bond J-coupling ($^1J_{CC} \approx 35$ Hz) between the ith $^{13}C^{methyl}$ and jth $^{13}C^{aliphatic}$ nuclei, remains close to unity ($\sim 0.6-0.9$) for the maximum value of t_{1b} used ($\sim 4-8$ ms) and therefore leads only to minor line broadening in the ^{15}N (F_1) dimension.[99]

C. 4D SCT-TEDOR pulse scheme

The 3D SCT-TEDOR scheme suppresses the modulation of $^{15}N-{}^{13}C^{methyl}$ cross peaks due to one-bond $^{13}C-{}^{13}C$ J-couplings and enables significant coherence transfer to be achieved via the weaker $^{15}N-{}^{13}C^{methyl}$ couplings, which, as discussed below, leads to sensitivity gains in many cases. Another major advantage of this scheme is that it can be trivially converted into a 4D NMR experiment without any additional sensitivity losses. This 4D SCT-TEDOR scheme is shown in Fig. 1(B). Briefly, placing the two central 180° pulses during the REDOR periods (black rectangles) on the ^{13}C channel instead of ^{15}N and moving them sequentially in t_{2a} and t_{2b} (with equal t_{2a} and t_{2b} increments), as shown in the figure, enables up to $2T$ (i.e., $\sim 16-24$ ms) of CT $^{13}C^{methyl}$ frequency encoding in t_2 ($t_2 = t_{2a} + t_{2b}$), which results in very high spectral resolution in the F_2 dimension. Immediately prior to the application of the 90° ^{13}C y-pulse at time point c, the relevant part of the density operator (assuming cosine modulated signal components in both t_1 and t_2) is given by

$$\rho(c) = 2C_{ix}\sin^2(\omega_{ij}\tau_{CN}/2)\prod_{k\neq j}\cos^2(\omega_{ik}\tau_{CN}/2) \times \cos(\pi^1 J^{ij}_{CC} t_{1b})\cos(\Omega_{N_j} t_1)\cos(\Omega_{C_i} t_2). \quad (13)$$

A fraction of the methyl ^{13}C magnetization can now be relayed to the directly bonded aliphatic ^{13}C nucleus (C_j) using a variety of magnetization transfer schemes[4,5] to further increase the spectral resolution (e.g., for a valine residue, the $^{15}N-{}^{13}C\gamma 1$ buildup trajectory as a function of τ_{CN} can be detected at both $^{13}C\gamma 1$ and $^{13}C\beta$ frequencies in the F_3 dimension). The resulting observable "diagonal" and "cross" signals giving rise to peaks at frequencies $[\Omega_{N_j},\Omega_{C_i},\Omega_{C_i}]$ and $[\Omega_{N_j},\Omega_{C_i},\Omega_{C_j}]$, respectively, in each of the 3D $^{15}N-{}^{13}C^{methyl}-{}^{13}C$ NMR spectra comprising the 4D SCT-TEDOR series are

$$S_{diag} \propto \langle \sin^2(\omega_{ij}\tau_{CN}/2)\prod_{k\neq j}\cos^2(\omega_{ik}\tau_{CN}/2)\rangle \cos(\pi^1 J^{ij}_{CC} t_{1b}) \times \exp(i\Omega_{N_j} t_1)\exp(i\Omega_{C_i} t_2)\exp(i\Omega_{C_i} t_3), \quad (14a)$$

$$S_{cross} \propto \langle \sin^2(\omega_{ij}\tau_{CN}/2)\prod_{k\neq j}\cos^2(\omega_{ik}\tau_{CN}/2)\rangle \cos(\pi^1 J^{ij}_{CC} t_{1b}) \times \exp(i\Omega_{N_j} t_1)\exp(i\Omega_{C_i} t_2)\exp(i\Omega_{C_j} t_3). \quad (14b)$$

We have investigated $^{13}C-{}^{13}C$ magnetization transfer using the double-quantum band-selective SPC-5_3 pulse sequence[54,108] as well as dipolar assisted rotational resonance (DARR)/rf-assisted spin diffusion (RAD) scheme.[83,115] With our experimental parameters, superior magnetization transfer was generally achieved with SPC-5_3 relative to DARR/RAD (e.g., in NAV the $^{13}C\gamma 1/\gamma 2-{}^{13}C\beta$ cross-peak volumes were $\sim 25\%-30\%$ of the corresponding diagonal peak volumes with 1.35 ms of SPC-5_3 mixing, whereas the cross-peak volumes were $\sim 6\%-10\%$ relative to the diagonal peaks with 5 ms of DARR/RAD).

D. Internuclear distance measurements in proteins

The internuclear $^{15}N-{}^{13}C^{methyl}$ distances in proteins can be determined from $^{15}N-{}^{13}C^{methyl}$ cross-peak buildup trajectories, using an implementation of the formalism described in detail in the context of previous 3D TEDOR experiments on small peptides.[52] According to Eqs. (11), (14a), and (14b), the intensities (volumes) of individual $^{15}N-{}^{13}C^{methyl}$ cross peaks are proportional to

$$I_{ij}(\tau_{CN}) \propto \langle \sin^2(\omega_{ij}\tau_{CN}/2)\prod_{k\neq j}\cos^2(\omega_{ik}\tau_{CN}/2)\rangle. \quad (15)$$

Note that due to the constant-time nature of the SCT-TEDOR experiments, the cross-peak buildup trajectories are purely dipolar in nature (i.e., not influenced by J-couplings or relaxation), with the main fit parameters being ω_{ij} (the active dipolar coupling) and ω_{ik} (passive couplings). Although, Eq. (15) appears to be quite simple, its direct use in the analysis of experimental TEDOR trajectories is complicated by the formal dependence on the relative orientation of $^{15}N-{}^{13}C$ dipolar couplings. To circumvent this problem, a simplified analytical formalism has been proposed,[52] which is based on Bessel function expansions of REDOR/TEDOR-type NMR signals developed by Mueller.[116] The zeroth order approximation to this Bessel function expansion, which neglects all orientation-dependent terms and abolishes the need for powder averaging, gives the following expression for the cross-peak intensity as a function of τ_{CN}:[52]

$$I_{ij}(\tau_{CN}) = \Lambda_i(1-[J_0(\sqrt{2}D_{ij}\tau_{CN})]^2) \times \prod_{k\neq j}(1+[J_0(\sqrt{2}D_{ik}\tau_{CN})]^2), \quad (16)$$

where $J_0(x)$ is a Bessel function of zeroth order, D_{ij} and D_{ik} are the active and passive $^{15}N-{}^{13}C^{methyl}$ dipolar coupling constants [Eq. (4)], and Λ_i is an overall cross-peak amplitude scaling factor. The utility of this analytical expression [relative to Eq. (15)] for simulating TEDOR buildup trajectories was investigated extensively,[52] indicating that the use of the approximate analytical model is the major source of error in determining $^{13}C-{}^{15}N$ distances in the 3–5 Å regime, with expected uncertainties typically on the order of approximately $\pm 10\%-15\%$ of the measured distance.

An additional simplification of this analytical model is used here to facilitate the extension of the SCT-TEDOR methods from small peptides to larger proteins. As discussed previously,[52] in the case of completely resolved $^{15}N-^{13}C$ spectra for small peptides, the $^{15}N-^{13}C$ cross-peak trajectory fitting routine involves *simultaneously* fitting a set of N trajectories corresponding to a particular ^{13}C nucleus with a set of N equations of the form given in Eq. (16), where the fit parameters correspond to the N $^{15}N-^{13}C$ dipolar couplings (the identity of the active and passive couplings is appropriately interchanged for the different cross peaks). It is clear that this approach is likely to be problematic in larger systems since in most cases one or more of the N $^{15}N-^{13}C$ cross peaks corresponding to a particular ^{13}C nucleus will, at least partially, overlap with cross peaks corresponding to a different ^{13}C nucleus with a similar resonance frequency. Therefore, for systems with a potential for a significant cross-peak overlap, such as proteins, the fitting of individual cross-peak trajectories (rather than sets of cross-peak trajectories) to Eq. (16) promises to be the most generally applicable approach. Moreover, since the initial cross-peak buildup rate is most sensitive to the magnitude of the active dipolar coupling (the presence of passive couplings affects mainly the overall trajectory amplitude and evolution at longer mixing times), performing several successive fits of a particular cross-peak trajectory where the number of passive couplings (i.e., fit parameters) is systematically increased was found to give good results as far as the estimation of the active dipolar coupling was concerned (i.e., the initial fit involved only two parameters, Λ and D_{active}, followed, if necessary, by fits of Λ, D_{active}, $D_{passive,1}$; Λ, D_{active}, $D_{passive,1}$, $D_{passive,2}$; etc.). For a set of $^{15}N-^{13}C^{methyl}$ distance measurements in GB1, we found that in most cases, fitting only Λ and D_{active} (i.e., ignoring the passive couplings altogether) was sufficient to obtain reasonable fits. Moreover, in all the cases where significant discrepancies were observed (particularly at longer evolution times) between the experimental data and the Λ, D_{active} fit (referred to also as the *IS* model), an IS_2 model (i.e., the three-parameter, Λ, D_{active}, $D_{passive,1}$, fit) was sufficient to obtain a very good agreement with experiment (note that, as discussed below, despite the generally higher quality fits for the IS_2 model, the distance estimates obtained with the *IS* and IS_2 models were typically within ~0.1–0.2 Å).

IV. RESULTS AND DISCUSSION

A. Relative sensitivity of SCT-TEDOR and ZF-TEDOR schemes

Given the relatively long (~30 ms) duration of the SCT-TEDOR schemes, one of the main concerns regarding their general utility is related to sensitivity. Here, we show that not only is the sensitivity of the SCT-TEDOR schemes comparable to ZF-TEDOR (Ref. 52) (which would already be useful given the superior resolution furnished by 4D SCT-TEDOR), but that in some cases the new methods can actually provide substantial (approximately twofold to threefold) gains in sensitivity relative to ZF-TEDOR.

The relative sensitivity of ZF- and SCT-TEDOR was investigated using both analytical simulations of nuclear spin

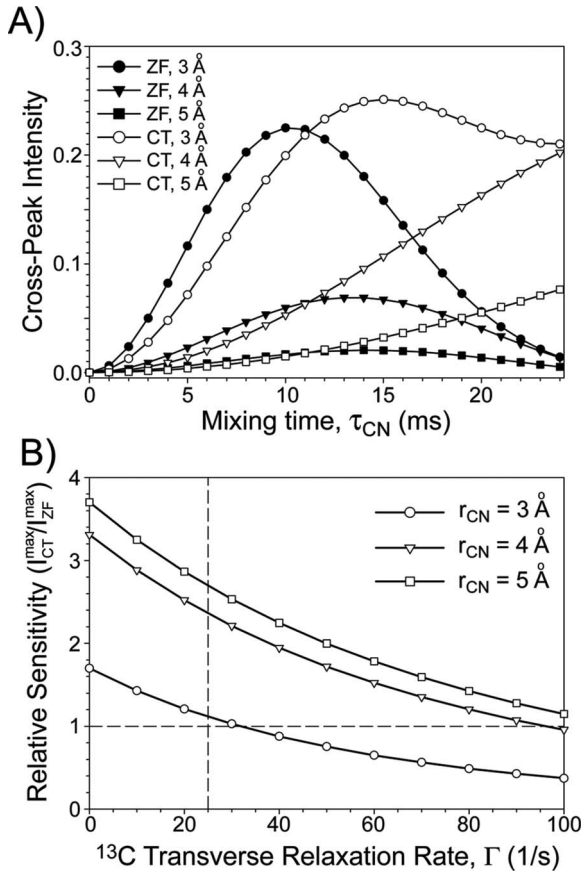

FIG. 2. Simulations of $^{15}N-^{13}C$ cross-peak trajectories and comparison of relative sensitivity of ZF-TEDOR (Ref. 52) and CT-TEDOR experiments, for typical distances involving *J*-coupled methyl ^{13}C for Ala, Ile, Leu, Val, and Thr residues in U-^{13}C, ^{15}N-labeled proteins. (A) Simulated $^{15}N-^{13}C$ cross-peak trajectories for ZF-TEDOR measurements corresponding to 3 Å (●), 4 Å (▼), and 5 Å (■) $^{15}N-^{13}C$ distances, and for CT-TEDOR measurements corresponding to 3 Å (○), 4 Å (▽), and 5 Å (□) $^{15}N-^{13}C$ distances, in the presence of one *J*-coupled ^{13}C nucleus (e.g., $^{13}C\alpha$ for Ala, $^{13}C\beta$ for Val, etc.). The cross-peak intensities are given as a fraction of the ^{13}C intensity in a 1D CPMAS experiment. For ZF-TEDOR, the analytical model (Ref. 52 and 116) (see text) was used to calculate cross-peak trajectories, further modulated by τ_{CN}-dependent terms describing the J_{CC} evolution of ^{13}C magnetization and transverse relaxation, i.e., $I_{ZF}(\tau_{CN}) = \frac{1}{2}(1-[J_0(\sqrt{2}D\tau_{CN})]^2)\cos^2(\pi^1 J_{CC}\tau_{CN}/2)\exp(-\Gamma\tau_{CN})$, with $^1J_{CC}=35$ Hz and $\Gamma=25$ s^{-1}. For CT-TEDOR, a similar expression was used, but with ^{13}C *J*-evolution and relaxation terms now corresponding to constants: $I_{CT}(\tau_{CN}) = |\frac{1}{2}(1-[J_0(\sqrt{2}D\tau_{CN})]^2)\cos(\pi^1 J_{CC}T_C)\exp(-\Gamma T_C)|$, with $^1J_{CC}=35$ Hz, $\Gamma=25$ s^{-1}, and $T_C=26.5$ ms (i.e., T_C is slightly shorter than the ideal value of $1/^1J_{CC}=28.7$ ms, which accounts for effects of ^{13}C transverse relaxation). Note that all simulations assume that ^{15}N transverse relaxation (expected to be significantly smaller than ^{13}C transverse relaxation) is negligible. (B) Calculated sensitivity of CT-TEDOR vs ZF-TEDOR experiments for the measurement of 3, 4, and 5 Å $^{15}N-^{13}C$ distances as a function of the ^{13}C transverse relaxation rate. The relative sensitivity is defined as the ratio $I_{CT}^{max}/I_{ZF}^{max}$, where I_{CT}^{max} and I_{ZF}^{max} are the maximum intensities observed in the calculated CT-TEDOR and ZF-TEDOR cross-peak trajectories, respectively. The analytical expressions above were used for the calculation of the individual trajectories. Note that for CT-TEDOR the optimal value of T_C depends on the relaxation rate, Γ therefore, in our approach, the optimal T_C for each value of Γ was first obtained from the evolution of the magnetization for a methyl ^{13}C spin *J*-coupled to one other ^{13}C, with $^1J_{CC}=35$ Hz calculated using $I(t)=\cos(\pi^1 J_{CC}t)\exp(-\Gamma t)$ (the optimal T_C values were between 28.7 and 21.9 ms for Γ in the 0 to 100 1/s range). Furthermore, for CT-TEDOR simulations, we considered τ_{CN} in the range of 0–20 ms, which corresponds to typical experimental values. The horizontal dashed line at the value $I_{CT}^{max}/I_{ZF}^{max}=1$ indicates the point where the sensitivities of the two experiments are equal. The vertical dashed line at the value $\Gamma=25$ s^{-1} indicates the experimentally determined transverse relaxation rate for methyl ^{13}C in U–^{13}C, ^{15}N-labeled N-acetyl-valine.

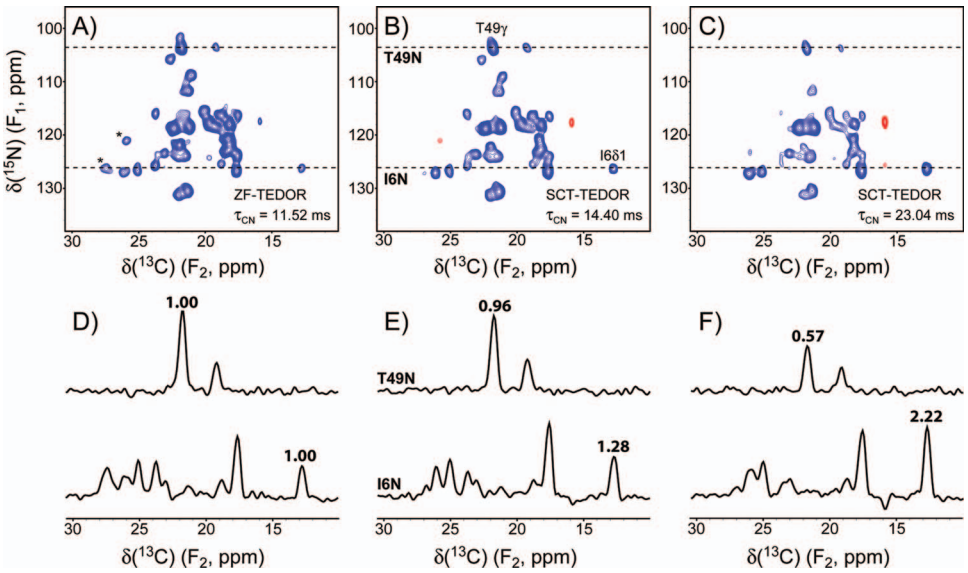

FIG. 3. (Color) Comparison of the relative sensitivity of ZF-TEDOR and SCT-TEDOR pulse schemes for the measurement of long-range $^{15}N-^{13}C^{methyl}$ distances in U$-^{13}C$, ^{15}N-labeled GB1. 2D $^{15}N-^{13}C^{methyl}$ chemical shift correlation spectra obtained using (A) ZF-TEDOR with $\tau_{CN}=11.52$ ms (Ref. 52), (B) SCT-TEDOR [scheme in Fig. 1(A)] with $\tau_{CN}=14.40$ ms, and (C) SCT-TEDOR with $\tau_{CN}=23.04$ ms. Asterisks in spectrum (A) denote lysine and leucine $^{15}N-^{13}C\gamma$ correlations, present in ZF-TEDOR spectra, but effectively suppressed in SCT-TEDOR due to the constant-time J-evolution. Each 2D spectrum was acquired as a 30^{*} $(t_1,{}^{15}N)\times 1000^{*}(t_2,{}^{13}C)$ data matrix with time increments of $(360,20)$ μs, acquisition times of (10.4,20.0) ms, and a total measurement time of ~2.7 h/spectrum. Positive (blue) and negative (red) cross peaks are drawn with the lowest contour levels at ten times the rms noise level. (D)–(F) One-dimensional slices from the 2D spectra in (A)–(C), taken at ^{15}N frequencies corresponding to residues T49 and I6 as indicated. Representative cross peaks in proteins associated with typical ~3 Å (T49N-T49γ) and ~4 Å (I6N-I6δ1) $^{15}N-^{13}C^{methyl}$ distances are highlighted, with the cross-peak intensities relative to those in the ZF-TEDOR spectrum indicated in the 1D slices in (D)–(F).

dynamics in simple three-spin model systems (consisting of a dipole-coupled $^{15}N-^{13}C$ pair, with the ^{13}C spin J-coupled to another ^{13}C with $^{1}J_{CC}=35$ Hz) and experiments in U$-^{13}C$, ^{15}N-labeled GB1. Figure 2(A) shows simulated cross-peak buildup trajectories for ZF- and CT-TEDOR for $^{15}N-^{13}C$ distances of 3, 4, and 5 Å. The simulations assume a typical $^{13}C^{methyl}$ transverse relaxation rate, $\Gamma=25$ s^{-1}, determined experimentally for methyl ^{13}C groups in NAV using spin-echo experiments (data not shown), under the MAS and ^{1}H decoupling conditions employed in this study (see figure caption for additional details). As expected,[52] the simulations indicate that ZF-TEDOR cross-peak trajectories are modulated by $^{13}C-^{13}C$ J-evolution, which for $^{1}J_{CC}=35$ Hz limits the useful $^{15}N-^{13}C$ coherence-transfer time (i.e., time where the maximum cross-peak intensity is achieved) to ~10–14 ms. On the other hand, due to the constant-time nature of the experiment, the CT-TEDOR trajectories are purely dipolar and free of such modulations. This enables significantly higher $^{15}N-^{13}C$ magnetization transfer at longer mixing times, especially for weak $^{15}N-^{13}C$ couplings corresponding to long-range distances (e.g., for a 4 Å $^{15}N-^{13}C$ distance, the CT-TEDOR cross-peak intensity for $\tau_{CN}=20$ ms is more than double the maximum value that can be achieved with ZF-TEDOR). We note here that the main underlying concept of SCT-TEDOR, namely, CT-type $^{15}N-^{13}C$ coherence transfer with concurrent $^{13}C^{methyl}$ evolution, could in principle also be implemented within the ZF-TEDOR scheme. Although this would produce purely dipolar τ_{CN} trajectories and enable a limited amount, up to ~6 ms, of "relaxation-free" $^{13}C^{methyl}$ encoding, both the resolution and the sensitivity of such a modified ZF-TEDOR scheme would still be inferior to the SCT-TEDOR experiments. A more extensive comparison of the relative sensitivity of ZF- and CT-TEDOR experiments is presented in Fig. 2(B), where we plot the relative sensitivity of the two experiments (defined here as the ratio of the maximum cross-peak intensity in CT- and ZF-TEDOR simulations, $I_{CT}^{max}/I_{ZF}^{max}$, obtained within the typical mixing time range $\tau_{CN}=0-20$ ms) as a function of the ^{13}C transverse relaxation rate for $^{15}N-^{13}C$ distances of 3, 4, and 5 Å. Remarkably, for almost all distance and ^{13}C relaxation rate combinations, CT-TEDOR is predicted to offer comparable or improved sensitivity relative to ZF-TEDOR. Indeed, only for $^{13}C-^{15}N$ distances <3 Å, which are associated with rapid cross-peak buildup (e.g., intraresidue $^{15}N-^{13}C\beta$ distances in alanine residues), and/or large Γ values (which would generally lead to poor experimental performance for either experiment) is the sensitivity superior for ZF-TEDOR. The predicted sensitivity gains for CT-TEDOR at practically all experimentally relevant ^{13}C transverse relaxation rates (i.e., $\Gamma\approx 10-40$ s^{-1}) are most significant (approximately twofold to threefold) for the most structurally interesting distances ($r_{CN}\approx 3.5-5$ Å) and are expected to increase further with more efficient ^{1}H decoupling (i.e., at smaller Γ values).

In order to test the theoretical predictions of Fig. 2, a series of 2D $^{15}N-^{13}C^{methyl}$ correlation spectra was recorded for GB1 using the different TEDOR mixing schemes. Figure 3 shows an optimized ZF-TEDOR spectrum acquired with a mixing time $\tau_{CN}\approx 11.5$ ms and SCT-TEDOR spectra recorded with mixing times of ~14.4 and 23 ms, optimized for highest cross-peak intensity for ~3 and 4 Å distances, respectively. While the cross peaks associated with two-bond Ala $^{15}N-^{13}C\beta$ couplings, i.e., $r_{CN}\approx 2.5$ Å (see Fig. 5 for

resonance assignments) are clearly more intense for ZF-TEDOR relative to SCT-TEDOR, this is not the case for signals corresponding to typical $^{15}N-^{13}C^{methyl}$ distances in the ~3–4 Å range. For example, the intensity of the T49N-T49γ correlation ($r_{CN} \approx 3$ Å) is approximately equal (within a few percent) in ZF-TEDOR and SCT-TEDOR ($\tau_{CN}=14.4$ ms) spectra, and the I6N-I6δ1 cross peak ($r_{CN} \approx 4$ Å) exhibits a greater than twofold intensity in the $\tau_{CN} \approx 23$ ms SCT-TEDOR spectrum relative to ZF-TEDOR. These experimental observations are in good agreement with the calculated cross-peak intensities in Fig. 2 and underscore the general utility of the SCT-TEDOR schemes for the measurement of long-range $^{15}N-^{13}C^{methyl}$ dipolar couplings in peptides and proteins.

B. SCT-TEDOR experiments on U–^{13}C, ^{15}N-labeled N-acetyl-valine

The 3D and 4D SCT-TEDOR experiments were first implemented using the model peptide, N-acetyl-valine, to probe the distances between the amide ^{15}N and $^{13}C\gamma1$ and $^{13}C\gamma2$ methyl groups and to optimize the $^{13}C-^{13}C$ magnetization transfer scheme and phase cycling (the Cγ1 and Cγ2 labels for NAV simply serve as an enumerating aid and do not imply stereospecific assignments). Figure 4 shows the results of the 4D SCT-TEDOR experiment on NAV, acquired with SPC-5_3 $^{13}C-^{13}C$ mixing.[54,108] Note that 3D SCT-TEDOR and 4D SCT-TEDOR-DARR mixing[83,115] data sets were also recorded (data not shown), giving essentially identical $^{15}N-^{13}C_\gamma$ dipolar couplings. (F_1,F_3) strips corresponding to small regions of a 3D $^{15}N-^{13}C^{methyl}$ correlation spectrum acquired with a REDOR mixing time $\tau_{CN} \approx 14$ ms, taken at F_2 frequencies corresponding to $^{13}C\gamma1$ and $^{13}C\gamma2$, are shown in Fig. 4(A) (see figure caption for experimental details). The $^{13}C-^{13}C$ diagonal peaks (e.g., N–Cγ1–Cγ1), as well as one-bond (e.g., N–Cγ1–Cβ) and two-bond (e.g., N–Cγ1–Cγ2) cross peaks, generated during the SPC-5_3 mixing period, are clearly observed. As expected, due to the double-quantum nature of SPC-5_3 $^{13}C-^{13}C$ mixing, the cross peaks display the characteristic sign-alternated pattern, with signals corresponding to one-bond transfers having opposite signs relative to the diagonal and the relayed transfers over two bonds having the same sign. Figure 4(B) shows representative trajectories for N–Cγ1–Cγ1 and N–Cγ1–Cβ peaks [highlighted by the dashed rectangles in Fig. 4(A)] as a function of the mixing time τ_{CN}. These trajectories, both of which report on the same $^{15}N-^{13}C\gamma1$ distance, were simulated using the analytical expression of Eq. (16) with a single active $^{13}C-^{15}N$ coupling (i.e., the *IS* model) resulting in best-fit distances of 3.01 and 3.14 Å for the N–Cγ1–Cγ1 and N–Cγ1–Cβ trajectories, respectively. Similar analysis of the N–Cγ2–Cγ2 and N–Cγ2–Cβ trajectories (data not shown) gave the best-fit $^{15}N-^{13}C\gamma2$ distance of 2.94 and 3.10 Å. These distance estimates are generally in good agreement with the NAV N–Cγ distances of 2.98 and 3.09 Å, determined by x-ray crystallography.[117]

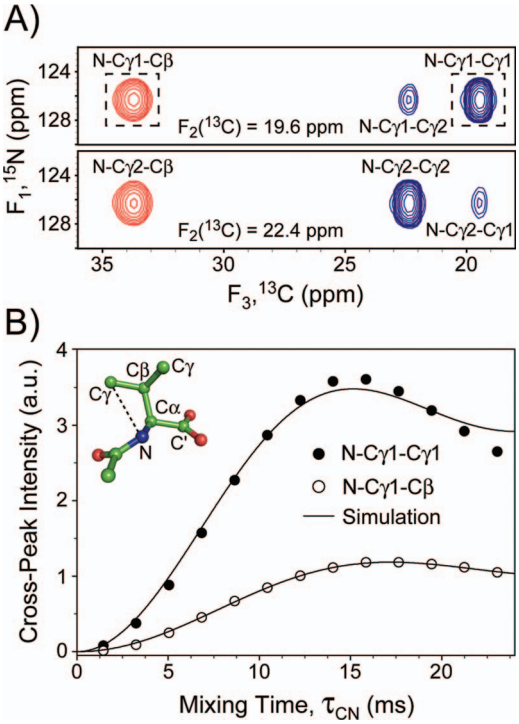

FIG. 4. (Color) 4D SCT-TEDOR experiment on N-acetyl-valine. (A) Small $^{15}N-^{13}C$ (F_1,F_3)-regions corresponding to the two $^{13}C\gamma$ resonances in the F_2 dimension, taken from a 3D $^{15}N-^{13}C^{methyl}-^{13}C$ correlation spectrum acquired using the pulse scheme in Fig. 1(B) with a REDOR mixing time τ_{CN} of 14.04 ms. The 4D experiment was acquired as a 8^* (t_1,^{15}N) $\times 32(t_2,^3C) \times 1000^*(t_3,^{13}C) \times 13(\tau_{CN})$ data matrix with time increments of (1440,720,20,1800) μs, resulting in acquisition times of (10.0,22.3,20.0,23.0) ms, and a total measurement time of ~37 h. Positive (blue) and negative (red) cross peaks are drawn with the lowest contour levels at 15 times the rms noise level. The cross-peak assignments are indicated, where Cγ1 and Cγ2 correspond to resonances at 19.6 and 22.4 ppm, respectively (note that these labels do not imply a stereospecific assignment of the Cγ resonances). (B) Representative trajectories of the absolute cross-peak intensity as a function of the mixing time τ_{CN} for N–Cγ1–Cγ1 (●) and N–Cγ1–Cβ (○) cross peaks in the series of 3D $^{15}N-^{13}C^{methyl}-^{13}C$ correlation spectra. Simulations using the analytical model of Eq. (16) with a single active $^{15}N-^{13}C$ coupling (see text for details) are also shown (—), which yielded the best-fit $^{15}N-^{13}C\gamma1$ distances of 3.01 Å (N–Cγ1–Cγ1) trajectory and 3.14 Å (N–Cγ1–Cβ trajectory).

C. SCT-TEDOR experiments on U–^{13}C, ^{15}N-labeled GB1

In this section, we demonstrate the utility of the SCT-TEDOR methods for the simultaneous determination of multiple $^{15}N-^{13}C^{methyl}$ distances in U–^{13}C, ^{15}N-labeled proteins, using the 56-residue GB1 as a model system. The 3D SCT-TEDOR experiment was performed on GB1 with the REDOR mixing time τ_{CN} varied between ~3 and 23 ms, and the results are summarized in Fig. 5. Figure 5(A) shows a 2D $^{15}N-^{13}C^{methyl}$ correlation spectrum of GB1 (corresponding to the $\tau_{CN}=14.4$ ms slice of the 3D), with the major cross peaks indicated (the assignments have been obtained using the published chemical shifts,[15] and a total of 21 well-resolved cross peaks could be readily identified for the 33 methyl groups present in GB1). The signal-to-noise ratio for the SCT-TEDOR data acquired on the ~1.5 μmol GB1 sample was such that each 2D spectrum in the 3D series could be acquired in only ~2.7 h (i.e., the entire 3D was recorded in ~21.5 h). This bodes quite well for the extension of this

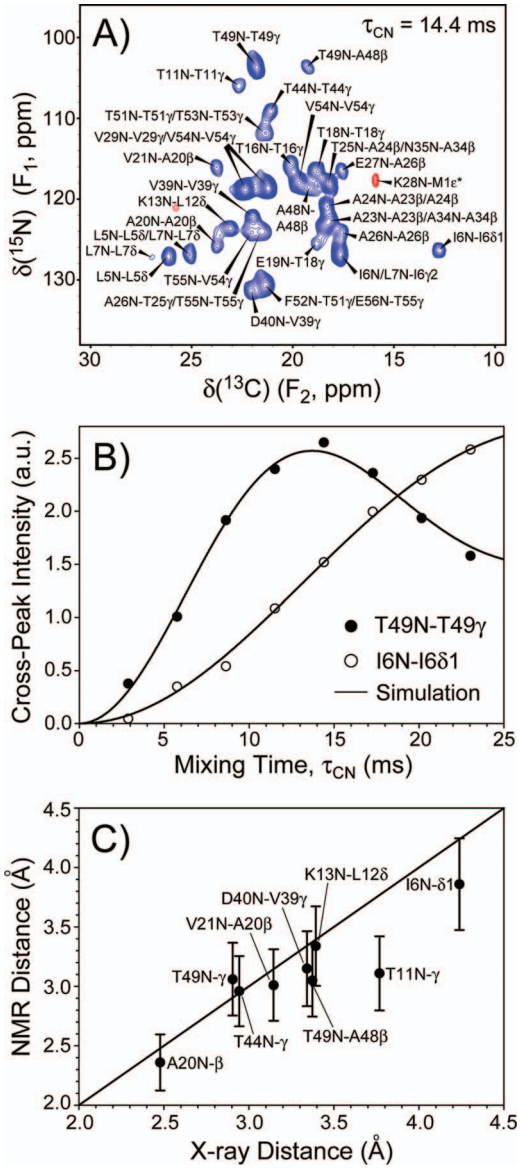

FIG. 5. (Color) 3D SCT-TEDOR experiment on GB1. (A) A two-dimensional slice from the 3D SCT-TEDOR experiment, corresponding to the $^{15}N-^{13}C^{methyl}$ chemical shift correlation spectrum, recorded with a REDOR mixing time τ_{CN} of 14.4 ms. The 3D SCT-TEDOR spectrum was acquired as a 30^{*} $(t_1, ^{15}N)\times 1000^{*}(t_2, ^{13}C)\times 8(\tau_{CN})$ data matrix with time increments of (360,20,2880) μs, resulting in acquisition times of (10.4,20.0,23.0) ms and a total measurement time of ~21.5 h. Positive (blue) and negative (red) cross peaks are drawn with the lowest contour levels at ten times the rms noise level. The resonance assignments are based on published ^{13}C and ^{15}N chemical shifts for GB1 (Ref. 15) and a 3D $^{15}N-^{13}C^{methyl}-^{13}C$ correlation spectrum acquired with a REDOR mixing time of 15.84 ms [i.e., a slice from a 4D SCT-TEDOR experiment; see, Figs. 1(B) and 7]. The K28N-M1ε correlation (indicated by an asterisk) appears to result from an intermolecular contact between protein molecules in the GB1 microcrystals (Fig. 9). (B) Representative trajectories of cross-peak intensity as a function of τ_{CN} for T49N-T49γ (●) and I6N-I6δ1 (○) cross peaks, corresponding to $^{15}N-^{13}C$ distances in the ~3–4 Å range. Best-fit simulations using the IS_2 analytical model described in the text are also shown (—) (see Fig. 6 for additional experimental and simulated cross-peak trajectories). (C) Comparison of selected $^{15}N-^{13}C$ distances in GB1 determined using x-ray diffraction and 3D SCT-TEDOR (Table I). The uncertainties in the NMR distances (error bars of ±10% of the best-fit distance estimate are indicated in the figure) are associated primarily with the use of the approximate analytical model to describe the cross-peak trajectories (Ref. 52).

methodology to smaller samples and/or larger proteins, especially when higher B_0 fields and MAS rates, and more efficient ^{1}H decoupling and polarization transfer schemes[112,113] are employed to further enhance the overall experimental sensitivity. Note also that due to the constant-time nature of SCT-TEDOR, correlations not involving ^{13}C methyl groups, which would normally appear in the same spectral region [e.g., lysine and leucine $^{15}N-^{13}C\gamma$; see Fig. 3(A)], are effectively suppressed without the use of frequency-selective pulses or other spectral editing techniques.[52,101]

The 3D SCT-TEDOR experiment enabled us to analyze, in detail, the buildup trajectories for several cross peaks, which were well resolved in the 2D $^{15}N-^{13}C^{methyl}$ correlation spectrum. Specifically, we selected for the analysis a set of nine representative cross peaks (I6N-I6δ1, T11N-T11γ, K13N-L12δ, A20N-A20β, V21N-A20β, D40N-V39γ, T44N-T44γ, T49N-A48β, and T49N-T49γ) associated with $^{15}N-^{13}C^{methyl}$ distances in the range of ~2.5–4.5 Å in the x-ray structure of GB1 (PDB ID: 1pgb).[118] Note that although the current spectra do not provide the stereospecific assignments of Val Cγ and Leu Cδ *a priori*, the analysis of the GB1 crystal structure indicates that the K13N-L12δ and D40N-V39γ correlations of interest, which correspond to distances of ~3–3.5 Å, most likely involve the Lδ2 and Vγ1 carbons (the K13N-L12δ1 and D40N-V39γ2 distances are ~5.2 and 4.5 Å, respectively, and are expected to give rise to much weaker cross peaks in the range of the mixing times probed; see Fig. 2). The T49N-T49γ and I6N-I6δ1 trajectories shown in Fig. 5(B) clearly demonstrate the very different cross-peak buildup profiles associated with ~3 Å (T49N-T49γ) and ~4 Å (I6N-I6δ1) $^{15}N-^{13}C$ distances. The cross-peak trajectories were fitted using the analytical *IS* and IS_2 models described in Sec. III [the IS_2 fits are shown in Fig. 5(B)]. The experimental and simulated trajectories for all the cross peaks in the set are shown in Fig. 6, and the associated best-fit $^{15}N-^{13}C^{methyl}$ distances are summarized in Table I and compared with the corresponding x-ray distances in Fig. 5(C). It is interesting to note that the simplest *IS* model, which assumes only the presence of a single active dipolar coupling and is clearly a very rough approximation in many cases, provided initial fits of reasonable quality for most of the cross-peak trajectories. Specifically, this model was able to accurately reproduce the initial parts of the trajectories (Fig. 6), consistent with the idea that the initial rate of cross-peak buildup in TEDOR-type experiments is, in general, governed primarily by the magnitude of the active dipolar coupling. For those trajectories, where significant discrepancies between the experiment and *IS* fits were observed (e.g., V21N-A20β, T44N-T44γ, T49N-T49γ), the most pronounced deviations occurred at mixing times $\tau_{CN} \gtrsim 10-15$ ms. (Note that the A20N-A20β trajectory is associated with relatively poor-quality fits due to our choice of the mixing time increments, which were optimized for the measurement of ~3–5 Å distances. This trajectory is shown only to demonstrate the rapid cross-peak buildup observed for intraresidue two-bond $^{15}N-^{13}C$ dipolar couplings.) In these cases, the fit quality could be substantially improved by using the IS_2 model, which includes one additional passive coupling. Remarkably, despite the generally higher quality

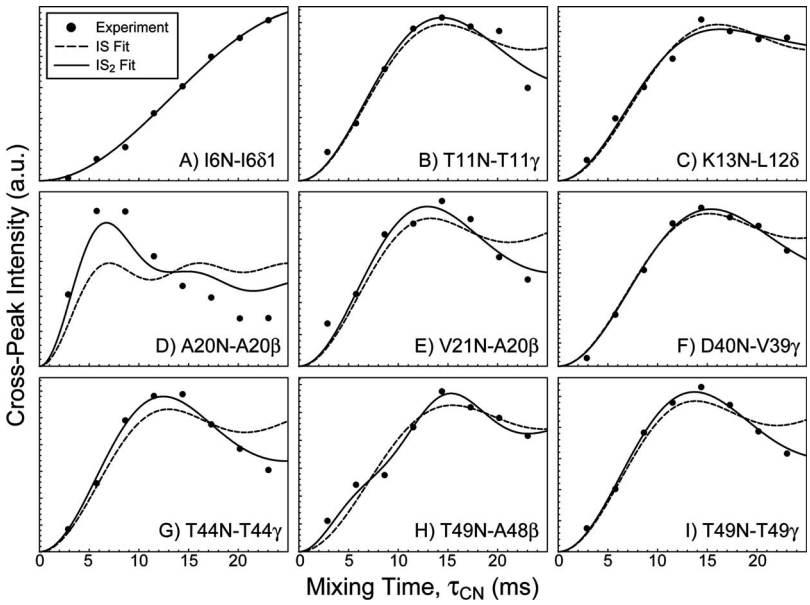

FIG. 6. Representative cross-peak trajectories as a function of the mixing time τ_{CN} from the 3D SCT-TEDOR experiment on U$-^{13}$C, ^{15}N-labeled GB1. The trajectories correspond to a set of nine cross peaks (indicated in the plots), which are well resolved in the 2D ^{15}N$-^{13}$C^{methyl} correlation spectrum [Fig. 5(A)]. Best-fit simulations using the *IS* (dotted lines) and IS_2 (solid lines) analytical models (see text for details) are also shown, and the best-fit distances are listed in Table I.

fits for the IS_2 model, most of the distance estimates obtained with the *IS* and IS_2 models were within ~0.1–0.2 Å (Table I). The inclusion of an additional passive coupling (i.e., the IS_3 model) was investigated for several of the cross peaks (data not shown) and was found to have little effect on the overall fit quality and the best-fit distances determined using the simpler simulation models.

A comparison of the ^{15}N$-^{13}$C^{methyl} distances in GB1 measured using 3D SCT-TEDOR, with the corresponding values in the published x-ray crystal structure (PDB ID: 1pgb)[118] reveals a reasonable agreement [Fig. 5(C)]. With the exception of the T11N-T11γ measurement (see discussion below), all ^{15}N$-^{13}$C^{methyl} distances determined by NMR are within $\sim\pm10\%$ of their x-ray counterparts, which we consider to be acceptable given the approximate nature of the data analysis and the fact that these longer-range ^{15}N$-^{13}$C^{methyl} distances are quite sensitive to the exact values of the intervening dihedral angles (i.e., in addition to the inherent experimental uncertainties, the minor differences between the NMR and x-ray distances may, at least in part, reflect subtle structural differences between protein single crystals and the microcrystals used for the SSNMR analysis). We now turn our attention to the T11N-T11γ measurement, which, relative to the other measurements, appears to deviate more substantially from 1pgb (SCT-TEDOR data yield a T11N-T11γ distance of ~3.1 Å, which differs by ~0.7 Å or ~20% from the x-ray distance of ~3.8 Å). The T11N-T11γ cross-peak trajectory [Fig. 6(B)] does not display any obvious anomalies and exhibits qualitatively the same features as the T44N-T44γ and T49N-T49γ ($r_{CN}\approx3$ Å) trajectories while differing markedly from the I6N-I6δ1 ($r_{CN}\approx4$ Å) trajectory. Therefore, it is indeed quite likely that different T11 side-chain $\chi1$ (i.e., N–Cα–Cβ–Oγ) rotamers are present in GB1 single crystals and in the microcrystalline protein preparation used in the current study. Given that Thr $\chi1=+60°$, 180°, and −60° rotamers correspond to intraresidue ^{15}N$-^{13}$Cγ distances of ~2.95, 2.95, and 3.8 Å, respectively, the SCT-TEDOR measurements are consistent with the presence of $\chi1\approx+60°$ and/or 180° T11 rotamers (instead of the $\chi1\approx-80°$ conformation present in 1pgb). Although additional SSNMR measurements would be required to unequivocally confirm the presence of the different $\chi1$ rotamers, this possibility is supported by several additional observations. First, the detailed analysis of the backbone dynamics of GB1 in solution[119] indicates that the loop between the $\beta1$- and $\beta2$-strands, which contains T11, is one of the most flexible regions of the protein (i.e., the conformational space accessible to T11 is larger than for residues found in regular secondary structure elements). Second, the inspection of orthorhombic and trigonal GB1 lattices[118] reveals that the T11 side chain is relatively isolated and does not appear to be obviously involved in critical intra- and intermolecular protein contacts. Finally, the analysis of 132 proteins of known structure containing nearly 1500 Thr residues,[120] shows that Thr $\chi1=+60°$ and −60° rotamers are most common, accounting for ~91% of the database ($\chi1=180°$ accounts for the remaining ~9%), and occur with nearly equal frequency (46% for $\chi1=+60°$ and 45% for $\chi1=-60°$). This indicates

TABLE I. Selected methyl ^{13}C$-^{15}$N distances in GB1.

Atoms	Distance[a] (Å)		
	NMR (*IS* model)	NMR (IS_2 model)	X-ray[b]
I6N–I6δ1	3.75	3.86	4.24
T11N–T11γ	2.97	3.11	3.77
K13N–L12δ	3.07	3.34	3.39[c]
A20N–A20β	2.33	2.36	2.48
V21N–A20β	2.88	3.01	3.15
D40N–V39γ	3.01	3.15	3.34[d]
T44N–T44γ	2.86	2.96	2.94
T49N–A48β	3.03	3.05	3.37
T49N–T49γ	2.92	3.06	2.91

[a]Uncertainties in the measured NMR distances, associated with the use of the approximate analytical simulation model, are expected to be on the order of approximately ±10%–15% of the measured distance (see text). (Ref. 52).
[b]PDB ID: 1pgb. (Ref. 118).
[c]K13N–L12δ2 distance in 1pgb (see text).
[d]D40N–V39γ1 distance in 1pgb.

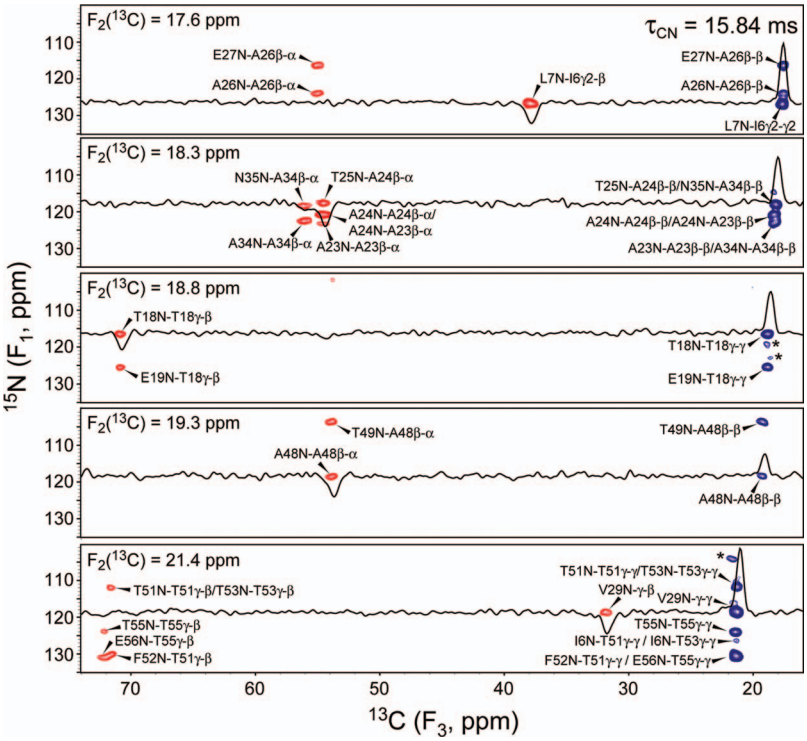

FIG. 7. (Color) (F_1,F_3)-regions taken from a 3D $^{15}N-^{13}C^{methyl}-^{13}C$ correlation spectrum of GB1 acquired using the pulse scheme in Fig. 1(B) with a RE-DOR mixing time τ_{CN} of 15.84 ms. The spectrum was acquired as a 30^* $(t_1,^{15}N)\times 181(t_2,^{13}C)\times 1000^*(t_3,^{13}C)$ data matrix with time increments of $(360,90,20)$ μs, resulting in acquisition times of $(10.4,16.2,20.0)$ ms, and a total measurement time of ~60 h. Positive (blue) and negative (red) cross peaks are drawn with the lowest contour levels at ten times the rms noise levels, and several selected one-dimensional F_3-traces are also shown. Peaks from adjacent F_2 planes are indicated by asterisks. Resonance assignments are based on the published ^{13}C and ^{15}N chemical shifts for GB1 (Ref. 15).

that the $\chi 1$ conformations, which are consistent with the measured $^{15}N-^{13}C\gamma$ distance for T11, are by no means unusual in proteins (indeed the $\chi 1=+60°$ conformation occurs with the highest frequency, albeit by a very small margin).

The 3D implementation of SCT-TEDOR allowed us to demonstrate the new methodology and perform a detailed analysis of several typical $^{15}N-^{13}C^{methyl}$ distances in GB1 (Figs. 5 and 6). In general, however, the resolution of 2D $^{15}N-^{13}C^{methyl}$ correlation spectra may not be sufficient, and the experiments will need to be performed in 4D mode (as shown in Fig. 4 for NAV). Although in this initial report we did not attempt the full 4D SCT-TEDOR experiment on GB1, in Fig. 7 we show a single slice of such a 4D experiment (i.e., a 3D $^{15}N-^{13}C^{methyl}-^{13}C$ correlation spectrum acquired with $\tau_{CN}\approx 16$ ms), which clearly demonstrates the advantages of increased spectral resolution offered by an independent $^{13}C^{methyl}$ frequency dimension followed by $^{13}C-^{13}C$ magnetization transfer. For example, in the $F_2=17.6$ ppm strip (top), the three signals with the same methyl ^{13}C frequency can be unambiguously separated in the F_3 dimension to yield a pair of cross peaks corresponding to A26β and a single correlation involving I6γ2. Note that the spectrum in Fig. 7 was acquired in ~60 h, which implies that with identical settings (i.e., full eight-step phase cycle and utilization of the entire CT period for $^{13}C^{methyl}$ encoding with minimal frequency aliasing in F_2), a 4D with four points in the τ_{CN} dimension could be recorded in ~10 days (while somewhat lengthy, this experiment duration is not absolutely prohibitive). Moreover, given that the experiment is of a constant-time variety and the spectral sensitivity was not the limiting factor in this case, the total experiment time could be significantly reduced (to ~5–7 days) by reducing the phase cycle to four steps and/or optimizing F_1 and F_2 aliasing (alternatively, additional τ_{CN} points could be recorded within a 4D experiment with a total duration of ~7–10 days).

Due to the characteristic magnitude of the $^{13}C-^{15}N$ dipolar coupling constants, TEDOR-type experiments are ideally suited to the measurements of $^{13}C-^{15}N$ distances up to ~5 Å [a 5 Å $^{13}C-^{15}N$ distance corresponds to $D\approx 25$ Hz; see Eq. (4)]. Given that for many proteins a typical methyl ^{13}C site will be in such proximity to ~2–3 ^{15}N nuclei (Fig. 8), these experiments will generally be very sensitive reporters of local backbone and side-chain conformation. Never-

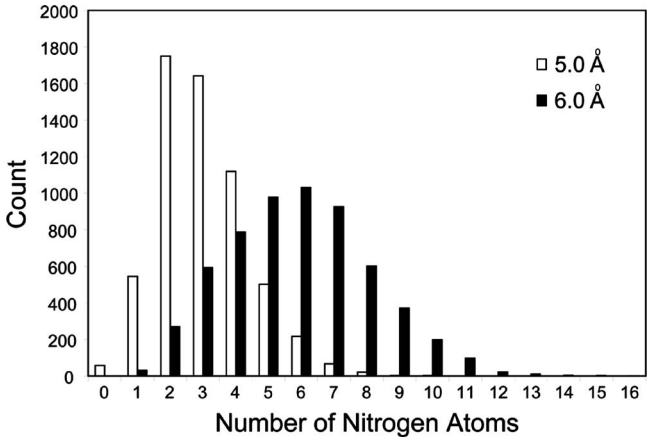

FIG. 8. Number of nitrogen atoms within a sphere of 5.0 or 6.0 Å radius around an Ala, Ile, Leu, Met, Val, or Thr methyl carbon in a database of 78 globular proteins of known structure (total of 5926 methyl groups). The protein database used corresponds to that employed by the TALOS program (Ref. 39) to predict protein secondary structure based on NMR chemical shifts. For ~75% of the methyl groups, two to four nitrogen atoms are found within a 5.0 Å radius, and the number of nitrogen neighbors increases rapidly when the radius is extended to 6 Å, resulting in a relatively broad distribution with the most probable value of 6.

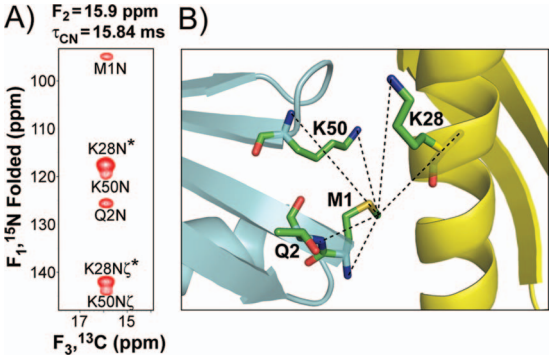

FIG. 9. (Color) (A) Small (F_1,F_3)-region taken from the 3D $^{15}N-^{13}C^{methyl}-^{13}C$ correlation spectrum of GB1 (Fig. 7) at the M1ε frequency in F_2, showing the correlations between M1ε and the neighboring ^{15}N nuclei. Six cross peaks were observed in this region and assigned based on the GB1 ^{13}C and ^{15}N chemical shifts (Ref. 15), combined with the analysis of the published GB1 crystal structures (Ref. 118). The four intramolecular correlations correspond to dipolar contacts between M1ε and M1N (NH_3^+), Q2N, K50N, and K50Nζ, and the two remaining cross peaks (indicated by asterisks) have been assigned to intermolecular contacts with K28N and K28Nζ. Note that the cross peaks corresponding to M1N and the lysine Nζ groups are folded in the F_1 dimension. (B) Structural model of GB1 in the trigonal lattice (PDB ID: 1pgb) (Ref. 118), which qualitatively accounts for the observed cross-peak pattern, with the relevant M1ε-N distances indicated by dotted lines. The neighboring GB1 molecules in the crystal lattice are shown in ribbon representation in cyan and yellow, and residues M1, Q2, K50, and K28 are shown in stick representation (the atom types for these residues are colored as follows: C=green, O=red, N=blue, S=yellow).

theless, in certain cases involving isolated protein molecules, and certainly for supramolecular peptide and protein aggregates,[91,92] these $^{15}N-^{13}C^{methyl}$ contacts can provide valuable long-range structural information for residues far removed in the primary protein sequence. For GB1, the analysis of the 3D $^{15}N-^{13}C^{methyl}-^{13}C$ spectrum (Fig. 7) immediately revealed two such instances. First, the slice at F_2 =21.4 ppm (bottom of Fig. 7), which corresponds to the T51γ and T53γ frequency contains a relatively weak, but clearly discernible, correlation at the ^{15}N frequency associated with I6 (note that L5 and L7 ^{15}N also resonate in this region). The GB1 structure[118] reveals that this cross peak (or group of cross peaks) is most likely the result of the proximity of the β1- and β4-strands, containing residues I6 and T51/T53, respectively (the relevant distances are ~4.75, 4.9, and 5.1 Å for T53γ-I6N, T51γ-I6N, and T51γ-L5N, respectively). In addition, the region of the spectrum corresponding to M1ε and shown in Fig. 9(A) reveals six distinct $^{15}N-^{13}C$ cross peaks (note that these peaks can already be detected in a 2D $^{15}N-^{13}C^{methyl}$ correlation spectrum [see, Fig. 5(A)] recorded with a sufficiently high signal-to-noise ratio). Based on the published GB1 ^{13}C and ^{15}N chemical shifts,[15] combined with the analysis of the available GB1 crystal structures,[118] four of the observed cross peaks were assigned to intramolecular contacts between M1ε and M1N (NH_3^+), Q2N, K50N, and K50Nζ, and the remaining two cross peaks were associated with intermolecular contacts (the microcrystals used in this study consisted of 100% $U-^{13}C$, ^{15}N GB1) to K28N and K28Nζ, as shown in the qualitative structural model in Fig. 9(B). The identification of the intermolecular contacts was possible only by assuming that GB1 is present in the microcrystals in a trigonal lattice (PDB ID: 1pgb),[118] which packs the α-helix of one GB1 molecule in the vicinity of the N-terminus of another GB1 molecule. No significant intermolecular M1ε-^{15}N contacts at the observed frequencies could be identified when an orthorhombic lattice (1pga)[118] was assumed. Subsequent experiments in our laboratory, involving the measurements of methyl-methyl contacts in GB1 (Helmus[123]), as well as detailed studies of different GB1 crystal polymorphs[124] lend further support to the assumption of a trigonal lattice for GB1 microcrystals. Note also, that since the M1 side-chain is highly unlikely to adopt the same conformation in GB1 microcrystals and single crystals used for X-ray analysis, when performing the cross-peak assignments we considered primarily the observed ^{15}N frequencies followed by the general proximity of the M1 residue to other residues (as opposed to the precise distances between M1ε and individual ^{15}N nuclei).

V. CONCLUSIONS

We have described 3D and 4D SCT-TEDOR experiments, which enable the measurement of multiple long-range $^{15}N-^{13}C^{methyl}$ dipolar couplings in uniformly ^{13}C, ^{15}N-labeled peptides and proteins with high resolution and sensitivity. The new methods take advantage of characteristic ^{13}C spin topologies of side-chain methyl groups in amino acids alanine, isoleucine, leucine, methionine, threonine, and valine to encode $^{15}N-^{13}C^{methyl}$ dipolar coupling, ^{15}N, and/or $^{13}C^{methyl}$ chemical shift information within a single semiconstant-time evolution period, while concurrently suppressing the modulation of NMR coherences due to *J*-couplings and transverse relaxation. These approaches simultaneously offer significant (approximately twofold to threefold) sensitivity gains for measurements of $^{15}N-^{13}C$ dipolar couplings corresponding to long-range ($\gtrsim$3.5 Å) distances as well as increased spectral resolution. Moreover, the resulting $^{15}N-^{13}C^{methyl}$ cross-peak trajectories are purely dipolar in nature, which enables the straightforward extraction of the relevant distances using analytical models of spin dynamics. The SCT-TEDOR experiments were demonstrated on a uniformly ^{13}C, ^{15}N-labeled peptide, N-acetyl-valine, and a 56-residue protein, GB1, highlighting the utility of the measured $^{15}N-^{13}C^{methyl}$ dipolar couplings for providing atomic-resolution, site-specific information about side-chain dihedral angles and the packing of protein molecules in the crystal lattice. Based on the sensitivity observed in the GB1 studies, this methodology should be readily applicable to other peptide and protein systems.

ACKNOWLEDGMENTS

This research was supported by the Ohio State University. We thank Professor Chad M. Rienstra (University of Illinois, Urbana-Champaign) for the gifts of samples of $U-^{13}C$, ^{15}N-labeled N-acetyl-valine and a control sample of $U-^{13}C$, ^{15}N-labeled GB1 and Dr. Angela M. Gronenborn (University of Pittsburgh) for the gift of the plasmid encoding for GB1. We also thank Professor Chad M. Rienstra and Professor Thomas J. Magliery (Ohio State University) for stimulating discussions.

[1] A. E. McDermott, Curr. Opin. Struct. Biol. **14**, 554 (2004).
[2] R. W. Martin, E. K. Paulson, and K. W. Zilm, Rev. Sci. Instrum. **74**, 3045 (2003).
[3] J. A. Stringer, C. E. Bronnimann, C. G. Mullen, D. H. H. Zhou, S. A. Stellfox, Y. Li, E. H. Williams, and C. M. Rienstra, J. Magn. Reson. **173**, 40 (2005).
[4] S. K. Straus, Philos. Trans. R. Soc. London, Ser. B **359**, 997 (2004).
[5] C. E. Hughes and M. Baldus, Annu. Rep. NMR Spectrosc. **55**, 121 (2005).
[6] H. B. R. Cole, S. W. Sparks, and D. A. Torchia, Proc. Natl. Acad. Sci. U.S.A. **85**, 6362 (1988).
[7] R. W. Martin and K. W. Zilm, J. Magn. Reson. **165**, 162 (2003).
[8] J. Pauli, B. van Rossum, H. Forster, H. J. M. de Groot, and H. Oschkinat, J. Magn. Reson. **143**, 411 (2000).
[9] A. McDermott, T. Polenova, A. Bockmann, K. W. Zilm, E. K. Paulsen, R. W. Martin, and G. T. Montelione, J. Biomol. NMR **16**, 209 (2000).
[10] J. Pauli, M. Baldus, B. van Rossum, H. de Groot, and H. Oschkinat, ChemBioChem **2**, 272 (2001).
[11] A. Bockmann, A. Lange, A. Galinier, S. Luca, N. Giraud, M. Juy, H. Heise, R. Montserret, F. Penin, and M. Baldus, J. Biomol. NMR **27**, 323 (2003).
[12] T. I. Igumenova, A. E. McDermott, K. W. Zilm, R. W. Martin, E. K. Paulson, and A. J. Wand, J. Am. Chem. Soc. **126**, 6720 (2004).
[13] A. J. van Gammeren, F. B. Hulsbergen, J. G. Hollander, and H. J. M. de Groot, J. Biomol. NMR **31**, 279 (2005).
[14] D. Marulanda, M. L. Tasayco, M. Cataldi, V. Arriaran, and T. Polenova, J. Phys. Chem. B **109**, 18135 (2005).
[15] W. T. Franks, D. H. Zhou, B. J. Wylie, B. G. Money, D. T. Graesser, H. L. Frericks, G. Sahota, and C. M. Rienstra, J. Am. Chem. Soc. **127**, 12291 (2005).
[16] A. Lange, S. Becker, K. Seidel, K. Giller, O. Pongs, and M. Baldus, Angew. Chem., Int. Ed. **44**, 2089 (2005).
[17] G. Pintacuda, N. Giraud, R. Pierattelli, A. Bockmann, I. Bertini, and L. Emsley, Angew. Chem., Int. Ed. **46**, 1079 (2007).
[18] A. Goldbourt, B. J. Gross, L. A. Day, and A. E. McDermott, J. Am. Chem. Soc. **129**, 2338 (2007).
[19] P. S. Nadaud, J. J. Helmus, and C. P. Jaroniec, Biomol. NMR Assign. **1**, 117 (2007).
[20] C. M. Rienstra, L. Tucker-Kellogg, C. P. Jaroniec, M. Hohwy, B. Reif, T. Lozano-Perez, B. Tidor, and R. G. Griffin, Proc. Natl. Acad. Sci. U.S.A. **99**, 10260 (2002).
[21] F. Castellani, B. van Rossum, A. Diehl, M. Schubert, K. Rehbein, and H. Oschkinat, Nature (London) **420**, 98 (2002).
[22] S. G. Zech, A. J. Wand, and A. E. McDermott, J. Am. Chem. Soc. **127**, 8618 (2005).
[23] C. P. Jaroniec, C. E. MacPhee, V. S. Bajaj, M. T. McMahon, C. M. Dobson, and R. G. Griffin, Proc. Natl. Acad. Sci. U.S.A. **101**, 711 (2004).
[24] K. Iwata, T. Fujiwara, Y. Matsuki, H. Akutsu, S. Takahashi, H. Naiki, and Y. Goto, Proc. Natl. Acad. Sci. U.S.A. **103**, 18119 (2006).
[25] M. Etzkorn, A. Bockmann, A. Lange, and M. Baldus, J. Am. Chem. Soc. **126**, 14746 (2004).
[26] D. Marulanda, M. L. Tasayco, A. McDermott, M. Cataldi, V. Arriaran, and T. Polenova, J. Am. Chem. Soc. **126**, 16608 (2004).
[27] E. K. Paulson, C. R. Morcombe, V. Gaponenko, B. Dancheck, R. A. Byrd, and K. W. Zilm, J. Am. Chem. Soc. **125**, 14222 (2003).
[28] V. Chevelkov, K. Faelber, A. Diehl, U. Heinemann, H. Oschkinat, and B. Reif, J. Biomol. NMR **31**, 295 (2005).
[29] A. Lesage, L. Emsley, F. Penin, and A. Bockmann, J. Am. Chem. Soc. **128**, 8246 (2006).
[30] N. Giraud, M. Blackledge, M. Goldman, A. Bockmann, A. Lesage, F. Penin, and L. Emsley, J. Am. Chem. Soc. **127**, 18190 (2005).
[31] M. Hologne, K. Faelber, A. Diehl, and B. Reif, J. Am. Chem. Soc. **127**, 11208 (2005).
[32] J. L. Lorieau and A. E. McDermott, J. Am. Chem. Soc. **128**, 11505 (2006).
[33] A. T. Petkova, Y. Ishii, J. J. Balbach, O. N. Antzutkin, R. D. Leapman, F. Delaglio, and R. Tycko, Proc. Natl. Acad. Sci. U.S.A. **99**, 16742 (2002).
[34] C. Ritter, M. L. Maddelein, A. B. Siemer, T. Luhrs, M. Ernst, B. H. Meier, S. J. Saupe, and R. Riek, Nature (London) **435**, 844 (2005).
[35] H. Heise, W. Hoyer, S. Becker, O. C. Andronesi, D. Riedel, and M. Baldus, Proc. Natl. Acad. Sci. U.S.A. **102**, 15871 (2005).
[36] A. Lange, K. Giller, S. Hornig, M. F. Martin-Eauclaire, O. Pongs, S. Becker, and M. Baldus, Nature (London) **440**, 959 (2006).
[37] Y. Li, D. A. Berthold, H. L. Frericks, R. B. Gennis, and C. M. Rienstra, ChemBioChem **8**, 434 (2007).
[38] M. Hiller, L. Krabben, K. R. Vinothkumar, F. Castellani, B. J. van Rossum, W. Kuhlbrandt, and H. Oschkinat, ChemBioChem **6**, 1679 (2005).
[39] G. Cornilescu, F. Delaglio, and A. Bax, J. Biomol. NMR **13**, 289 (1999).
[40] H. Heise, K. Seidel, M. Etzkorn, S. Becker, and M. Baldus, J. Magn. Reson. **173**, 64 (2005).
[41] L. L. Chen, R. A. Olsen, D. W. Elliott, J. M. Boettcher, D. H. H. Zhou, C. M. Rienstra, and L. J. Mueller, J. Am. Chem. Soc. **128**, 9992 (2006).
[42] M. Schubert, T. Manolikas, M. Rogowski, and B. H. Meier, J. Biomol. NMR **35**, 167 (2006).
[43] M. Baldus, A. T. Petkova, J. Herzfeld, and R. G. Griffin, Mol. Phys. **95**, 1197 (1998).
[44] M. Hong, J. Magn. Reson. **139**, 389 (1999).
[45] V. Ladizhansky, C. P. Jaroniec, A. Diehl, H. Oschkinat, and R. G. Griffin, J. Am. Chem. Soc. **125**, 6827 (2003).
[46] W. T. Franks, B. J. Wylie, S. A. Stellfox, and C. M. Rienstra, J. Am. Chem. Soc. **128**, 3154 (2006).
[47] J. D. Gehman, E. K. Paulson, and K. W. Zilm, J. Biomol. NMR **27**, 235 (2003).
[48] A. E. Bennett, R. G. Griffin, and S. Vega, in *Solid State NMR IV: Methods and Applications of Solid-State NMR*, edited by B. Blumich (Springer-Verlag, Berlin, 1994), Vol. 33, p. 1.
[49] S. Dusold and A. Sebald, Annu. Rep. NMR Spectrosc. **41**, 185 (2000).
[50] L. M. McDowell and J. Schaefer, Curr. Opin. Struct. Biol. **6**, 624 (1996).
[51] F. A. Kovacs, D. J. Fowler, G. J. Gallagher, and L. K. Thompson, Concepts Magn. Reson. **30A**, 21 (2007).
[52] C. P. Jaroniec, C. Filip, and R. G. Griffin, J. Am. Chem. Soc. **124**, 10728 (2002).
[53] A. Grommek, B. H. Meier, and M. Ernst, Chem. Phys. Lett. **427**, 404 (2006).
[54] M. Hohwy, C. M. Rienstra, C. P. Jaroniec, and R. G. Griffin, J. Chem. Phys. **110**, 7983 (1999).
[55] P. Hodgkinson and L. Emsley, J. Magn. Reson. **139**, 46 (1999).
[56] V. Ladizhansky and S. Vega, J. Chem. Phys. **112**, 7158 (2000).
[57] D. P. Raleigh, M. H. Levitt, and R. G. Griffin, Chem. Phys. Lett. **146**, 71 (1988).
[58] K. Takegoshi, K. Nomura, and T. Terao, Chem. Phys. Lett. **232**, 424 (1995).
[59] P. R. Costa, B. Q. Sun, and R. G. Griffin, J. Am. Chem. Soc. **119**, 10821 (1997).
[60] P. T. F. Williamson, A. Verhoeven, M. Ernst, and B. H. Meier, J. Am. Chem. Soc. **125**, 2718 (2003).
[61] R. Ramachandran, V. Ladizhansky, V. S. Bajaj, and R. G. Griffin, J. Am. Chem. Soc. **125**, 15623 (2003).
[62] V. Ladizhansky and R. G. Griffin, J. Am. Chem. Soc. **126**, 948 (2004).
[63] A. K. Paravastu and R. Tycko, J. Chem. Phys. **124**, 194303 (2006).
[64] I. Marin-Montesinos, G. Mollica, M. Carravetta, A. Gansmuller, G. Pilelo, M. Bechmann, A. Sebald, and M. H. Levitt, Chem. Phys. Lett. **432**, 572 (2006).
[65] A. E. Bennett, C. M. Rienstra, P. T. Lansbury, and R. G. Griffin, J. Chem. Phys. **105**, 10289 (1996).
[66] C. A. Michal and L. W. Jelinski, J. Am. Chem. Soc. **119**, 9059 (1997).
[67] T. Gullion and C. H. Pennington, Chem. Phys. Lett. **290**, 88 (1998).
[68] C. P. Jaroniec, B. A. Tounge, C. M. Rienstra, J. Herzfeld, and R. G. Griffin, J. Am. Chem. Soc. **121**, 10237 (1999).
[69] O. Liivak and D. B. Zax, J. Chem. Phys. **115**, 402 (2001).
[70] A. K. Mehta and J. Schaefer, J. Magn. Reson. **163**, 188 (2003).
[71] C. P. Jaroniec, B. A. Tounge, J. Herzfeld, and R. G. Griffin, J. Am. Chem. Soc. **123**, 3507 (2001).
[72] A. Lange, S. Luca, and M. Baldus, J. Am. Chem. Soc. **124**, 9704 (2002).
[73] B. Reif, B. J. van Rossum, F. Castellani, K. Rehbein, A. Diehl, and H. Oschkinat, J. Am. Chem. Soc. **125**, 1488 (2003).
[74] R. Tycko and Y. Ishii, J. Am. Chem. Soc. **125**, 6606 (2003).
[75] S. Balayssac, I. Bertini, M. Lelli, C. Luchinat, and M. Maletta, J. Am. Chem. Soc. **129**, 2218 (2007).
[76] P. S. Nadaud, J. J. Helmus, N. Hofer, and C. P. Jaroniec, J. Am. Chem. Soc. **129**, 7502 (2007).
[77] J. Cavanagh, W. J. Fairbrother, A. G. Palmer, and N. J. Skelton, *Protein NMR Spectroscopy: Principles and Practice* (Academic, San Diego, 1996).
[78] T. Gullion, D. B. Baker, and M. S. Conradi, J. Magn. Reson. (1969-1992) **89**, 479 (1990).

[79] N. Sinha, K. Schmidt-Rohr, and M. Hong, J. Magn. Reson. **168**, 358 (2004).
[80] T. Gullion and J. Schaefer, Adv. Magn. Reson. **13**, 57 (1989).
[81] A. W. Hing, S. Vega, and J. Schaefer, J. Magn. Reson. (1969-1992) **96**, 205 (1992).
[82] V. Tugarinov and L. E. Kay, ChemBioChem **6**, 1567 (2005).
[83] C. R. Morcombe, V. Gaponenko, R. A. Byrd, and K. W. Zilm, J. Am. Chem. Soc. **126**, 7196 (2004).
[84] S. G. Zech, E. Olejniczak, P. Hajduk, J. Mack, and A. E. McDermott, J. Am. Chem. Soc. **126**, 13948 (2004).
[85] P. McCaldon and P. Argos, Proteins **4**, 99 (1988).
[86] M. Eilers, S. C. Shekar, T. Shieh, S. O. Smith, and P. J. Fleming, Proc. Natl. Acad. Sci. U.S.A. **97**, 5796 (2000).
[87] I. T. Arkin and A. T. Brunger, Biochim. Biophys. Acta **1429**, 113 (1998).
[88] M. B. Ulmschneider and M. S. P. Sansom, Biochim. Biophys. Acta **1512**, 1 (2001).
[89] J. Janin, S. Miller, and C. Chothia, J. Mol. Biol. **204**, 155 (1988).
[90] R. Sprangers and L. E. Kay, Nature (London) **445**, 618 (2007).
[91] A. T. Petkova, W. M. Yau, and R. Tycko, Biochemistry **45**, 498 (2006).
[92] T. Sato, P. Kienlen-Campard, M. Ahmed, W. Liu, H. L. Li, J. I. Elliott, S. Aimoto, S. N. Constantinescu, J. N. Octave, and S. O. Smith, Biochemistry **45**, 5503 (2006).
[93] A. Bax, G. W. Vuister, S. Grzesiek, F. Delaglio, A. C. Wang, R. Tschudin, and G. Zhu, Methods Enzymol. **239**, 79 (1994).
[94] L. Mueller, J. Am. Chem. Soc. **101**, 4481 (1979).
[95] A. Bax, M. Ikura, L. E. Kay, D. A. Torchia, and R. Tschudin, J. Magn. Reson. (1969-1992) **86**, 304 (1990).
[96] J. C. Madsen and O. W. Sorensen, J. Magn. Reson. (1969-1992) **100**, 431 (1992).
[97] G. W. Vuister and A. Bax, J. Am. Chem. Soc. **115**, 7772 (1993).
[98] S. R. Van Doren and E. R. P. Zuiderweg, J. Magn. Reson., Ser. B **104**, 193 (1994).
[99] S. Grzesiek, H. Kuboniwa, A. P. Hinck, and A. Bax, J. Am. Chem. Soc. **117**, 5312 (1995).
[100] M. A. McCoy, J. Magn. Reson. **130**, 341 (1998).
[101] S. Jehle, M. Hiller, K. Rehbein, A. Diehl, H. Oschkinat, and B. J. van Rossum, J. Biomol. NMR **36**, 169 (2006).
[102] A. Bielecki and D. P. Burum, J. Magn. Reson., Ser. A **116**, 215 (1995).
[103] A. Pines, M. G. Gibby, and J. S. Waugh, J. Chem. Phys. **59**, 569 (1973).
[104] G. Metz, X. Wu, and S. O. Smith, J. Magn. Reson., Ser. A **110**, 219 (1994).
[105] B. M. Fung, A. K. Khitrin, and K. Ermolaev, J. Magn. Reson. **142**, 97 (2000).
[106] E. L. Hahn, Phys. Rev. **80**, 580 (1950).
[107] D. Suter and R. R. Ernst, Phys. Rev. B **32**, 5608 (1985).
[108] M. Hohwy, C. M. Rienstra, and R. G. Griffin, J. Chem. Phys. **117**, 4973 (2002).
[109] A. E. Bennett, C. M. Rienstra, M. Auger, K. V. Lakshmi, and R. G. Griffin, J. Chem. Phys. **103**, 6951 (1995).
[110] R. R. Ernst, G. Bodenhausen, and A. Wokaun, *Principles of Nuclear Magnetic Resonance in One and Two Dimensions* (Clarendon, Oxford, 1987).
[111] C. P. Jaroniec, B. A. Tounge, C. M. Rienstra, J. Herzfeld, and R. G. Griffin, J. Magn. Reson. **146**, 132 (2000).
[112] K. Takegoshi and T. Terao, J. Chem. Phys. **117**, 1700 (2002).
[113] E. Fry, V. Phan, and K. W. Zilm, presented at the 48th Experimental Nuclear Magnetic Resonance Conference, Daytona Beach, FL, 2007.
[114] J. S. Hu and A. Bax, J. Biomol. NMR **9**, 323 (1997).
[115] K. Takegoshi, S. Nakamura, and T. Terao, Chem. Phys. Lett. **344**, 631 (2001).
[116] K. T. Mueller, J. Magn. Reson., Ser. A **113**, 81 (1995).
[117] P. J. Carroll, P. L. Stewart, and S. J. Opella, Acta Crystallogr. **C46**, 243 (1990).
[118] T. Gallagher, P. Alexander, P. Bryan, and G. L. Gilliland, Biochemistry **33**, 4721 (1994).
[119] J. J. Barchi, B. Grasberger, A. M. Gronenborn, and G. M. Clore, Protein Sci. **3**, 15 (1994).
[120] R. L. Dunbrack and M. Karplus, J. Mol. Biol. **230**, 543 (1993).
[121] D. J. States, R. A. Haberkorn, and D. J. Ruben, J. Magn. Reson. (1969-1992) **48**, 286 (1982).
[122] D. Marion and K. Wüthrich, Biochem. Biophys. Res. Commun. **113**, 967 (1983).
[123] J. J. Helmus (unpublished).
[124] H. L. Frericks-Schmidt, L. J. Sperling, Y. G. Gao, B. J. Wylie, J. M. Boettcher, S. R. Wilson, C. M. Rienstra, J. Phys. Chem. B (2007), ASAP article (doi: 10.1021/jp075531p).